

## MIT Open Access Articles

*Phlogopite- and clinopyroxene-dominated fractional crystallization of an alkaline primitive melt: petrology and mineral chemistry of the Dariv Igneous Complex, Western Mongolia*

The MIT Faculty has made this article openly available. **Please share** how this access benefits you. Your story matters.

**Citation:** Bucholz, Claire E., Oliver Jagoutz, Max W. Schmidt, and Oyungerel Sambuu. "Phlogopite- and clinopyroxene-dominated fractional crystallization of an alkaline primitive melt: petrology and mineral chemistry of the Dariv Igneous Complex, Western Mongolia." *Contributions to Mineralogy and Petrology* 167:4 (2014 Mar 27):article 994.

**As Published:** <http://dx.doi.org/10.1007/s00410-014-0994-6>

**Publisher:** Springer Berlin Heidelberg

**Persistent URL:** <http://hdl.handle.net/1721.1/103591>

**Version:** Author's final manuscript: final author's manuscript post peer review, without publisher's formatting or copy editing

**Terms of use:** Creative Commons Attribution-Noncommercial-Share Alike



# Phlogopite- and Clinopyroxene-dominated Fractional Crystallization of an Alkaline Primitive Melt: Petrology and Mineral Chemistry of the Dariv Igneous Complex, Western Mongolia

Claire E. Bucholz<sup>1\*</sup>, Oliver Jagoutz<sup>2</sup>, Max W. Schmidt<sup>3</sup>, Oyungerel Sambuu<sup>4</sup>

<sup>1</sup>*Massachusetts Institute of Technology/Woods Hole Oceanographic Institution Joint Program in Oceanography, Cambridge, MA 02139, USA*

<sup>2</sup>*Department of Earth, Atmospheric, and Planetary Sciences Massachusetts Institute of Technology, Cambridge, MA 02139, USA*

<sup>3</sup>*Department of Earth Sciences, ETH, 8092 Zürich, Switzerland*

<sup>4</sup>*Mongolian University of Science & Technology, School of Geology and Petroleum Engineering, Ulaanbaatar, Mongolia*

\*Corresponding Author:

Dept. of Earth, Atmospheric and Planetary Sciences, 54-1020

Massachusetts Institute of Technology

77 Massachusetts Avenue

Cambridge, MA 02139-4307

Tel.: +1 (617) 452-2784,

E-mail Address: cbucholz@mit.edu

## Abstract

We present field relationships, petrography, and mineral major and trace element data for the Neoproterozoic Dariv Igneous Complex of the Altai of Western Mongolia. This unique complex of high-K plutonic rocks is composed of well-exposed, km-scale igneous intrusions of wehrlites, phlogopite wehrlites, apatite-bearing phlogopite clinopyroxenites, monzogabbros, monzodiorites, and clinopyroxene-bearing monzonites, all of which are intruded by late stage lamprophyric and aplitic dikes. The biotite-dominated igneous complex intrudes depleted harzburgitic serpentinite. The observed lithological variability and petrographic observations suggest that the plutonic rocks can be ascribed to a fractionation sequence defined by olivine + clinopyroxene  $\pm$  Fe-Ti oxides  $\rightarrow$  phlogopite + apatite  $\rightarrow$  K-feldspar + plagioclase  $\rightarrow$  amphibole + quartz. Notably, phlogopite is the dominant hydrous mafic mineral. Petrogenesis of the observed lithologies through a common fractionation sequence is supported by a gradual decrease in the Mg# (molar Mg/(Fe<sub>total</sub> + Mg) x 100) of mafic minerals. Crystallization conditions are derived from experimental phase petrology and mineral chemistry. The most primitive ultramafic cumulates crystallized at  $\leq 0.5$  GPa and 1210-1100°C and oxygen fugacity ( $f_{O_2}$ ) of +2-3  $\Delta$ FMQ (log-units above the fayalite-quartz-magnetite buffer). Trace element modeling using clinopyroxene and apatite REE compositions indicates that the dominant mechanism of differentiation was fractional crystallization. The trace element composition of a parental melt was calculated from primitive clinopyroxene compositions and compares favorably with the compositions of syn-magmatic lamprophyres that cross-

cut the fractionation sequence. The parental melt composition is highly enriched in Th, U, large ion lithophile elements (LILE), and light rare earth elements (LREE) and has a pronounced negative Nb-Ta depletion, suggestive of an alkaline primitive melt originating from a subduction-imprinted mantle. Comparison to a global compilation of primitive arc melts demonstrates that Dariv primitive melts are similar in composition to high-K primitive melts found in some continental arcs. Thus, the high-K fractionation sequence exposed in the Dariv Igneous Complex may be a previously unrecognized important fractionation sequence resulting in alkali-rich upper crustal granitoids in continental arc settings.

**Key Words:** high-K basalt; Dariv Range, Mongolia; fractionation sequence; biotite

## Introduction

Trace element similarities between subduction zone igneous rocks, bulk arc, and bulk crust estimates (e.g., enrichment in light REE, depletion in Nb and Ti, and enrichment of Pb) suggest that subduction-related magmatism is the main contributor to the present-day continental crust (CC) (e.g., Jagoutz and Schmidt 2012; Rudnick and Fountain 1995). Studying the generation and subsequent modification of arc primitive melts is therefore essential to understand the formation of the continental crust. After extraction from the mantle, primitive arc-related melts can either erupt at the surface or, more commonly, crystallize at depth, giving rise to ultramafic and mafic cumulates and residual melts. The phases that crystallize from the melts and their order of appearance depends on external parameters such as P, T, and  $f_{O_2}$ , but also strongly on the composition of the primitive melt. Primitive arc magmas fall into three broad compositional categories: 1) high-Mg andesites, 2) tholeiitic/calc-alkaline basalts, and 3) basalts with alkaline affinity (Tatsumi et al. 2008). Crystallization of tholeiitic/calc-alkaline magmas and high-Mg andesites at arc crustal conditions have been studied experimentally (e.g., Alonso-Perez et al. 2009; Grove et al. 2003; Sisson and Grove 1993) and in the field (e.g., Greene et al. 2006; Jagoutz et al. 2011; Jagoutz 2010), yet the fractionation of primitive alkali-rich basalts remains poorly defined. In part, the reason for the paucity of studies on alkaline basalt differentiation in arcs is the lack of field exposure and the limited, fragmentary evidence from cumulate xenoliths. Currently, the primary evidence of alkali-basalt fractionation arises from phlogopite-bearing ultramafic xenoliths in alkali-basalts and lamprophyres, which indicate that the fractionation sequence involves the crystallization of olivine + clinopyroxene + phlogopite  $\pm$  apatite (Buhlmann et al. 2000; Dawson and Smith 1992; Downes et al. 2004; Giannetti 1982; Giannetti and Luhr 1990; Righter and Rosas-Elguera 2001). Experimental phase-equilibria of hydrous alkali-rich magmas corroborate the limited evidence from high-K ultramafic xenoliths (Barton and Hamilton 1978; Barton and Hamilton 1979; Edgar et al. 1980; Elkins-Tanton and Grove 2003; Esperança and Holloway 1987; Melzer and Foley 2000; Righter and Carmichael 1996), yet, until now, an exposed, continuous plutonic sequence documenting such a fractionation sequence has not been described.

Here we present results from a newly discovered alkaline fractionation sequence in the Dariv Range of Western Mongolia. The Dariv Igneous Complex consists of a ~10 km thick sequence of high-K lithologies ranging from phlogopite-bearing ultramafic cumulates situated in a harzburgitic mantle to

feldspar-bearing monzogabbros, monzodiorites, and quartz-monzonites. As such, this series represents an unparalleled opportunity to constrain the crystallization conditions of a primitive, high-K, arc-related basalt. We describe field observations, petrology, and mineral chemistry (major and trace element) of this unique plutonic sequence with the aim of constraining the pressure, temperature, H<sub>2</sub>O content, and  $f_{O_2}$  during the crystallization of the alkali-rich parental melt. We present a detailed map of the northern plutonic sequence of the Dariv range, which is based on a total of 10 weeks of field work distributed over four field seasons (for a map documenting the areas visited see the online Supplementary Material) and then was completed based on satellite images. Field mapping and satellite images analysis has been done iteratively such that any uncertainties on the satellite images have been verified in the field. We also calculate the trace element composition of a primitive, parental melt composition to the high-K igneous complex that compares favorably with late stage syn-magmatic mafic dikes that cross-cut the alkaline complex. We then compare the primitive melt composition to a global compilation of primitive arc melts and model the incompatible element composition of the primitive melt in terms of a partial melt of the mantle and a component derived from a subducted slab.

### **Geological Setting and Previous Work**

The Dariv Range is located in southwestern Mongolia and is part of the Mongolian Altai (Fig. 1a). The Mongolian Altai are part of the Central Asian Orogenic Belt (CAOB), a massive subduction complex that extends from the Urals to the Pacific Ocean and from the Siberian and Baltic cratons to the North China and Tarim cratons. The CAOB is comprised of island arcs, ophiolites, accretionary wedges, and continental fragments that were accreted to the margin of Siberia beginning at *c.* 1.0 Ga and continuing until *c.* 250 Ma, when the Paleo-Asian ocean closed along the Solonker suture (Buslov et al. 2001; Khain et al. 2003; Sengör et al. 1993; Sengör et al. 1994). The CAOB contributed ~5.3 million km<sup>2</sup> of land area to Asia, strongly augmenting the temporal crustal growth curve during the Neoproterozoic and Paleozoic (Sengör et al. 1993). The Dariv Range exposes the contact between what we refer to as the Altai Allochthon, which is locally composed of high-grade Proterozoic metamorphic rocks (amphibolite- to granulite-facies meta-igneous and metasedimentary lithologies), and the Lake Terrane (an Ediacaran-Early Paleozoic island arc system) (Fig. 1b) (Badarch et al. 2002). The Lake Terrane is part of an extensive island-arc terrane composed of ophiolites and arc-related plutonic and volcanic rocks, which preserves fragments of the Palaeoasian ocean floor and associated island arc systems (Khain et al. 2003). In Dariv, the Lake Terrane is composed of six primary units: (1) a mantle section (serpentinized harzburgite and dunite), which is intruded by (2) an alkaline series ranging from phlogopite-rich mafic and ultramafic cumulates to alkaline granitoids, that together are the focus of this study. In addition, (3) an ophiolite sequence (gabbro, dike complex, and lavas) intrudes and lies structurally above the mantle section to the northwest (Fig. 1c, 2). The northern and western parts of the range are comprised of the (4) Lake Zone volcanics and volcanoclastics, poorly studied weakly metamorphosed igneous and sedimentary rocks (agglomerates, conglomerates, volcanics, and volcanoclastic rocks). Lastly, (5) a series of

hornblendites, hornblende-gabbros and –diorites and (6) large red (alkali-)granites that intrude (1), (2), and (5) are also present. The few previous studies of the area have not recognized the hydrous cumulate sequences, but have rather considered them part of the larger Dariv Ophiolite (also referred to as ‘Bayannur’ or ‘Bayannor’) ophiolite (Dijkstra et al. 2006; Khain et al. 2003; Kozakov et al. 2002).

The relatively complete igneous section of the ophiolite sequence (following the Penrose prototype) (Conference Participants 1972) suggests an origin at an oceanic spreading ridge. In addition, its location within the Lake Terrane implies that it formed in an oceanic environment. Dijkstra et al., (2006), however, identified geochemical characteristics that include Nb-Ta depletions and enrichment in LILE and suggested that this ophiolite formed in an arc environment and not a mid-ocean spreading center (Dijkstra et al. 2006). Calculated melt compositions in equilibrium with clinopyroxene from the ophiolitic gabbro-norites have trace element signatures similar to that of boninites and island-arc tholeiites (Dijkstra et al. 2006). The ophiolite has thus been postulated to have formed in a fore-arc environment (Dijkstra et al. 2006; Khain et al. 2003). The polarity of subduction and the overall structure of the Dariv Range, however, are debated and not well constrained. Dijkstra et al. (2006) interpret the area as a stack of steeply south-dipping thrust sheets, with the ophiolite being tectonically overlain by meta-sedimentary and meta-igneous rocks, and argue for a south-dipping subduction zone. In contrast, Khain et al. (2003) conclude that the ophiolite was thrust over the Dariv metamorphic complex in a subduction zone dipping to the north (Khain et al. 2003). This latter model is in agreement with the classical model of Sengör et al. (1993; 1994) of a long-lived north-facing subduction zone. The polarity of subduction, however, is still an open question that requires a more rigorous investigation of field relationships, structural data, and geochronology.

### **Field Relationships**

Several prominent west-northwest to east-southeast and northwest-southeast fault zones post date and cross cut the igneous and metamorphic sequences (Fig. 1c, 2). Our field mapping indicates that the units of the metamorphic sequence dip steeply ( $\sim 80^\circ$ ) to the south, but they are juxtaposed with the northern igneous sequence along high angle dextral faults rather than thrust faults. Their original thrusting relationship to the metamorphic sequence in the north, if any, is thus obscured. The field relationships of the ophiolite, the alkaline fractionation sequence, and the mantle section are described in greater detail below. Except for the ophiolite sequence, these lithologies are very fresh and do not display evidence of pervasive hydrous alteration as would be expected if the intrusion experienced the same regional fluid flux that lead to the complete serpentinization of the harzburgitic mantle. Consequently, it appears that the granitoids and the cumulates post-date and are not responsible for the serpentinization.

### **Alkaline Fractionation Sequence**

A  $\sim 3.5$  km thick biotite-bearing, ultramafic cumulate sequence is found within the harzburgite/dunite. The contact between the serpentinite and the cumulate sequence is marked by

numerous fingers filled with cumulate minerals that cut into the serpentinite (Fig. 2c, 4a). A broadly systematic lithological variation is observed from northwest to southeast in present-day reference frame (Fig. 2c). In the northwest primitive wehrlites characterized by bright green Cr-diopside, olivine, and minor phlogopite grade into clinopyroxenites, phlogopitites, and phlogopite monzogabbros towards the southeast. A detailed profile across part of the cumulate sequence was studied and sampled to document the mineralogical and geochemical changes associated with the systematic lithological variation that could represent progressive fractionation (Fig. 4). Lithological layering in the cumulate sequence in this detailed profile dips shallowly to the east-northeast. Late stage 10-100 cm wide K-feldspar-rich aplite dikes and mafic lamprophyre dikes with biotite phenocrysts cross cut the cumulate sequence (Fig. 3b,d, 4). Diffuse margins between the aplite dikes and the monzonites indicate a comagmatic origin (Fig. 3b), whereas the margins of mafic dikes are more sharply defined. Xenoliths of biotite cumulates and enclaves of mafic dikes are common in the monzonites (Fig. 3c,d). Volumetrically minor intrusions and veins of amphibole+clinopyroxene±biotite±feldspar bearing cumulates are also observed within the biotite-dominated cumulate sequence. In addition, the serpentinite is intruded by small (10-100 m in diameter) vertically oriented stocks of evolved granitoids and two large ~8 by 5 km wide intrusions of red (alkali-)granite (Fig. 2). The stocks are dominated by red (alkali-)granites and quartz monzonites, although other minor lithologies such as hornblende-bearing gabbros are also present. When observable, granitoid contacts with the serpentinite are defined by a fine-grained margin 10-20 cm thick.

### Ophiolite and Mantle Sequence

The ophiolite and mantle sequence combined are comprised from top to bottom of a dike complex, gabbro, and serpentinitized harzburgite and dunite, all overprinted by the same greenschist hydration/serpentinization event. The dikes are 1-2 m thick, fine-grained, and range in composition from basaltic andesites to rhyolites, with more felsic compositions becoming more common to the northwest. Plagioclase and augite phenocrysts are present in the basaltic andesite dikes, whereas porphyritic plagioclase and hornblende are occasionally present in the more evolved dikes. The dikes have variable orientations, striking southwest to northwest and dipping between 45 and 80°. The contact of the dike complex and the gabbro is transitional, with single dikes occasionally intruding the gabbro. The exposed gabbro sequence is 2-3 km thick and has limited modal mineral variations, consisting dominantly of 55% clinopyroxene + 45% plagioclase with a variable grain size of 0.1 to 1 cm. The gabbro intrudes the harzburgite and dunite along a steep (~210°/65°) igneous contact (Fig. 2b). The harzburgite and dunite are highly serpentinitized, but the serpentinitization was static as original textures are preserved. In thin section the harzburgites display a mesh texture of serpentine + brucite enclosing bastite pseudomorphs after orthopyroxene. The dunite generally occurs in decimeter- to meter-scale discordant veins in sharp contact with the harzburgite. The veins are vertically oriented and strike north-northwest. Chromium spinel is present in both the dunite and harzburgite.

## Petrography

As the focus of this study, the rocks comprising the biotite-rich alkaline fractionation sequence and associated (alkali-)granites are described in detail below. The rocks are generally very fresh, but occasionally clinopyroxene exhibits alteration to actinolitic amphibole. This is more pronounced in the monzodiorites and (qtz-)monzonites. None of the samples exhibit field or microstructural evidence of deformation. The modal mineralogy of representative samples is given in Table 1. Mineral percentages given in the following text are volume percentages.

### Wehrlites and Phlogopite Wehrlites

The wehrlites are fine- to medium-grained (0.5-2 mm). The most primitive (i.e., highest mineral and whole rock Mg#) phlogopite wehrlites consist of bright green clinopyroxene (~65%) and olivine (~25-30%) with intercumulus phlogopite (~2-10%) and occasional accessory titanomagnetite. Olivine occurs as subhedral to anhedral crystals that are poikilitically enclosed within phlogopite. In some samples, olivine shows highly irregular margins and is surrounded by phlogopite (Fig. 5a). Titanomagnetite (50-100  $\mu\text{m}$ ) grows along grain boundaries and within the rims of clinopyroxene. The modal percentage of biotite is variable in the wehrlites and gradually increases (to ~45%), while that of olivine and pyroxene decrease (to <10% and to ~45% respectively), resulting in a pronounced orthocumulate texture of olivine and clinopyroxene poikilitically enclosed within phlogopite (Fig. 5b). In one sample (MO-11-9) orthopyroxene occurs as sub- to euhedral crystals 0.5-1 mm in diameter as an orthocumulate phase with clinopyroxene or sometimes poikilitically enclosed by biotite.

### Phlogopite clinopyroxenites and phlogopitites

The phlogopite wehrlites grade into phlogopite clinopyroxenites that are comprised of clinopyroxene (70-80%), phlogopite (20-30%), and apatite with accessory hemo-ilmenite, titanite, and zircon. In the phlogopite clinopyroxenites, brown-reddish phlogopite grows interstitially to the clinopyroxene and occasionally completely encloses clinopyroxene (Fig. 5c,d). Titanite crystallizes in the rims of the phlogopites. In the one sampled phlogopitite (MO-11-10), phlogopite is the dominant phase (75%) and apatite becomes an important constituent (~4-5%). Phlogopite occurs both as an intercumulus phase and as elongate light brown euhedral laths up to 1-2 mm in length with subhedral clinopyroxene and stout prismatic apatites. Apatites are poikilitically enclosed by both euhedral and intercumulus biotite (Fig. 5d).

### Monzogabbros

Monzogabbros consist of alkali-feldspar and plagioclase (together 28-50%), phlogopite (13-25%), and clinopyroxene (31-55%) with accessory subhedral titanite, apatite, zircon, and hemo-ilmenite (Fig. 5e). Phlogopite grows both interstitially and in large laths (1-2 cm in length), occasionally poikilitically encloses titanite and apatite. Oligoclase to andesine (An ~20-40) and alkali-feldspar occur together in patchy intergrowths. Apatite occurs as stubby, subhedral 1-2 mm long crystals. Typically secondary green

actinolite partially replaces ~20% of both clinopyroxene and biotite.

#### Clinopyroxene-Bearing Monzodiorites and Quartz-Monzonites

The monzodiorites and quartz-monzonites are composed of large alkali-feldspar megacrysts with albite, quartz, biotite, amphibole, and clinopyroxene as major constituents and with accessory apatite, titanite, zircon, and hemo-ilmenite (Fig. 5f,g). In the quartz-monzonites, alkali-feldspars are large (1-2 cm in length) euhedral laths around which the other minerals grow. Quartz displays interlobate grain boundaries. Biotite occurs as stubby laths, 1-4 mm in length. Secondary green actinolite extensively replaces clinopyroxene. Clinopyroxene contains both biotite and numerous apatite inclusions (5-100  $\mu\text{m}$  diameter). Apatite is often also enclosed in biotite.

#### Lamprophyres

The late stage lamprophyre dikes that cross-cut the alkaline fractionation sequence are comprised of biotite, plagioclase, and clinopyroxene with accessory apatite, zircon, and hematite. Biotite (50%) occurs in 100-200  $\mu\text{m}$  long blocky laths often enclosing zircon and hematite. Subhedral, rounded 20-100  $\mu\text{m}$  clinopyroxene crystals (5%) are surrounded by plagioclase (45%). Plagioclase crystals display irregular margins and appear to have crystallized after biotite. Zircon is an abundant accessory phase occurring as 20-150  $\mu\text{m}$  long prismatic crystals within both plagioclase and biotite.

#### (Alkali-)Granites

The red (alkali-)granites consist of coarse-grained (>2 cm), strongly porphyritic K-feldspar phenocrysts (50%) surrounded by smaller crystals of quartz (30%), alkali-feldspar, plagioclase (15%), and biotite and amphibole (5%) with accessory zircon and titanite (Fig. 5h). The K-feldspar phenocrysts occasionally exhibit Carlsbad twinning with perthitic exsolution. Smaller K-feldspar grains often have tartan twinning. Quartz displays undulose extinction and has lobate grain boundaries.

#### Analytical Methods

The major element chemistry of minerals from 21 samples across the biotite-dominated fractionation sequence were determined by electron microprobe analysis (EMPA) using a JEOL JXA-8200 Superprobe at both the Massachusetts Institute of Technology and at ETH Zurich. An acceleration voltage of 15 kV, a beam current of 20 nA, and a beam diameter of 1-10  $\mu\text{m}$  were used. Measuring times were 40 s for all elements. Background counting time was half of the peak counting time. The CITZAF correction procedure of Armstrong (1995), including the atomic number correction, the absorption coefficients, and fluorescence correction therein, were used to reduce the data and obtain quantitative analyses. Detection limits are typically in the range of 0.02 to 0.05 wt %. Exceptions to this are detection limits for FeO and MnO of ~0.06 wt % and for F 0.09 wt %. Trace element chemistry of the minerals was determined using LA-ICP-MS at ETH Zurich. Samples were loaded along with the NIST610 glass standard in an ablation cell and the ablated material was transported to the ICP-MS by a He carrier gas.



The ablation system consists of a 193 nm ArF Excimer laser (Lambda Physik) with a homogenized beam profile connected to an Elan6100 DRC quadrupole ICP-MS. The background was measured for ~40s prior to each analysis and the laser signal was integrated over 40-50 s. A 40  $\mu\text{m}$  spot size was used and rims and cores of minerals were analyzed when possible. The analytical set-up was tuned for optimum performance across the entire mass range and daily optimization of the analytical conditions were performed to ensure a ThO production rate of below 0.2% (i.e. Th/ThO intensity ratio  $<0.002$ ) and a Th/U sensitivity ratio of 1 measured on the NIST610 glass standard. Two analyses on the NIST610 standard at the beginning and at the end of each set bracketed up to 20 analyses of unknowns. The NIST610 standard was used as an external standard to calibrate analyte sensitivities and to correct for a linear drift during a set of analyses. Data reduction of LA-ICP-MS analyses followed the procedures described in Longerich et al., (1996). CaO was used for clinopyroxene,  $\text{Al}_2\text{O}_3$  for phlogopite, and MgO for olivine as the internal standard element to correct for matrix effects and calculate trace element concentrations.

Four whole rock major and trace element compositions of mafic dikes are included in the presented data set. Fresh pieces with no indication of weathering or veining were cut from samples to ensure uncontaminated and representative chemical analyses. Samples were powdered in an agate mill, which was cleaned with silica sand in between samples. The powders were then oven-dried overnight at 105°C. Loss on ignition was determined from mass loss after heating in a 1050°C oven. Glass discs were prepared using lithium tetraborate as a flux during the fusion process. Major elements were measured using a wave-length dispersive X-ray fluorescence (XRF) spectrometer at ETH. Trace elements of the fusion discs were determined by laser ablation inductively coupled plasma mass spectrometer (LA-ICPMS) at ETH described above. In addition, a lithium tetraborate blank was measured at the beginning of each session and its spectrum subtracted from the unknown spectra. The XRF glass discs were broken and analyses were performed directly on freshly broken surfaces. Analytical procedures and data reduction are the same as described above for the mineral trace element analyses, except that a 90  $\mu\text{m}$  beam size was used. A minimum of 3 shots per disc in unique locations were done to examine homogeneity of the analyzed pellet. CaO was used as the internal standard element to correct for matrix effects and calculate trace element concentrations. CaO was used as the internal standard element to correct for matrix effects and calculate trace element concentrations.

### **Mineral Chemistry**

The average mineral major and trace element chemistry for individual samples of the biotite-dominated cumulate sequence are provided in the online Supplementary Material. The chemical characteristics of the primary fractionating minerals are described below.

#### **Olivine**

None of the serpentinite samples investigated preserved olivine such that all olivine can be ascribed to the magmatic suites. Olivine occurs as an early cumulate phase in the most primitive wehrlites and phlogopite wehrlites. Wehrlite olivines have an Mg# of 87-85 whereas the most primitive phlogopite

wehrlite has olivines  $Mg\# = 82-80$ . Compositional gaps observed in the  $Mg\#$  are likely an artifact of sampling. The transition from phlogopite wehrlites to olivine-free phlogopite clinopyroxenites is associated with a constant decrease in the modal percentage and  $Mg\#$  of olivine (down to  $Mg\# = 65$ ). Although variable, the NiO content of olivine generally decreases from 0.15-0.21 wt.% in the wehrlites to 0.07 to 0.15 wt.% in the phlogopite wehrlites (Fig. 6a). MnO contents of olivine increase with decreasing  $Mg\#$  from 0.18-0.2 in the wehrlites to 0.40 to 0.55 in the most evolved phlogopite wehrlites (Fig. 6b). Both the NiO and MnO contents for a given  $Mg\#$  of olivine are lower than typical average mantle olivine values (Sato 1977), indicating that the olivine is magmatic in origin and that the primitive melts may have already precipitated olivine-dominated cumulates (dunites). CaO contents are generally close to the detection limit of the electron microprobe.

### Clinopyroxene

Orthopyroxene is absent from the fractionation sequence except in one sample (MO-11-9). The ortho- and clinopyroxene in this sample, however, are severely out of Fe-Mg equilibrium with a  $K_D \approx 0.6$  (as compared to the empirically determined equilibrium value of  $1.09 \pm 0.14$ ) (Putirka 2008). The Fe-Mg equilibrium suggests instead that the orthopyroxene was originally olivine, which later through peritectic reaction with melt formed enstatite. Therefore, clinopyroxene appears to be the only fractionating pyroxene and remains a fractionating phase into the most evolved quartz-monzonites. Clinopyroxene's persistence as a crystallizing phase allows for its geochemical characterization across the entire fractionation sequence. The most magnesian clinopyroxenes in wehrlites have  $Mg\#$ 's of 89-91. The  $Mg\#$  of clinopyroxenes in phlogopite-bearing ultramafic cumulates vary between 80-88. Monzogabbro, monzodiorite, and monzonite clinopyroxene  $Mg\#$  values vary between ~60-75.  $Cr_2O_3$  contents decrease from values of 0.38-0.65 wt.% in the primitive wehrlites to <0.10 wt.% in the plagioclase-bearing lithologies.  $TiO_2$  increases with decreasing  $Mg\#$  before Fe-Ti oxides become a dominant crystallizing phase, and then dramatically declines (Fig. 6c). The  $Al_2O_3$  content of clinopyroxene generally increases with decreasing  $Mg\#$  in the cumulates lacking plagioclase and decreases once feldspar becomes a co-fractionating phase. This trend has been previously observed in pyroxenes from the Aleutian arc volcanic rocks (Kay and Kay 1985), from lower crustal cumulates (DeBari et al. 1987; Jagoutz et al. 2007), and in experimental studies on pyroxenites (Müntener et al. 2001). Some sub-solidus Tschermakitic exchange ( $(Fe,Mg)_2Si_{1-x}Al_x$ ) during cooling of clinopyroxene in the ultramafic cumulates is indicated by a decrease in clinopyroxene  $Al_2O_3$  contents with increasing  $Mg\#$  within individual samples (Fig. 6d).

The trace element characteristics of clinopyroxene (Fig. 7a) were determined for five phlogopite wehrlites (MO-10-323, MO-10-392, MO-10-394, MO-11-8, MO-11-9), one phlogopite clinopyroxenite (MO-10-325), one phlogopitite (MO-11-10), one monzogabbro (MO-11-12), three monzodiorites (MO-11-13, MO-11-14, MO-11-21) and one monzonite (MO-11-26). In general, the overall concentration of incompatible elements (except for Sr and Eu) in clinopyroxene increases by ~10x with progressive fractionation (Fig. 7a). Concentrations in a single grain are generally homogeneous, but some samples

show variations between core and rim concentrations with rims having slightly higher incompatible trace element concentrations. All clinopyroxenes are characterized by depletion in heavy rare earth elements (HREEs) relative to light rare earth elements (LREEs). This depletion becomes less pronounced with increasing fractionation ( $(\text{Ce}/\text{Yb})_N$  is ~5.8-9.0 in primitive phlogopite wehrlites and clinopyroxenites and ~2.9-4.3 in the monzogabbros, monzodiorites, and monzonites). Nb, Pb, Zr, and Hf are depleted in all clinopyroxenes across the entire fractionation sequence. Analyzed clinopyroxenes are also depleted in Sr except those from the most primitive analyzed wehrlite (MO-10-394). Eu is depleted with respect to neighboring REE in the monzogabbros, monzodiorites, and monzonites. This depletion becomes more pronounced with progressive fractionation. V concentrations in the clinopyroxenes increase from ~74 ppm in the most primitive phlogopite wehrlites to >360 ppm in the more evolved phlogopite clinopyroxenites. V concentrations in clinopyroxene from the plagioclase-bearing lithologies vary between 128-233 ppm.

### Biotite

The most primitive phlogopite wehrlites have biotites with Mg#’s of 85-88, whereas Mg#’s of biotite in the more evolved wehrlites decrease to ~70. The clinopyroxenites, phlogopitite, monzogabbros, monzodiorites, and monzonites have biotite Mg#’s of 67-73, 70-71, 57-62, 46-60, and 43-49, respectively. Biotites in the analyzed lamprophyre dike have Mg#’s of 59-65. The  $\text{Al}_2\text{O}_3$  contents of the biotite in the ultramafic cumulates (13.8-16.3 wt.%) and lamprophyre (13.9-16.8 wt.%) are generally higher than that in the mafic and more evolved lithologies (12.6-14.4 wt.%) (Fig. 6e).  $\text{TiO}_2$  contents are high and vary between 2.2-5.3 wt.% in the ultramafic cumulates and 3.4-4.6 wt.% in the feldspar-bearing lithologies. The  $\text{Na}_2\text{O}$  contents of biotite are variable within each sample, but generally decrease with decreasing Mg# from ~1.0 wt.% at Mg# ~85 to <0.1 wt.% at Mg# 45-50. Biotites in the feldspar bearing lithologies have uniformly low  $\text{Na}_2\text{O}$  (0.05-0.15 wt.%) (Fig. 6f). MnO increases with decreasing Mg# from 0-0.15 in the ultramafic cumulates to 0.12-0.33 in the monzogabbros through monzonites. Cl contents are below the detection limit (d.l.) in the ultramafic lithologies, but also vary between 0.07-0.12 wt.% in the feldspar-bearing lithologies. F contents are variable (<d.l. to 0.7 wt.%) and do not display any correlation with biotite Mg#.

Trace element analyses for biotite (Fig. 7b) were done on four phlogopite wehrlites (MO-10-323, MO-10-392, MO-10-394, MO-11-8), one phlogopite clinopyroxenite (MO-10-325), one phlogopitite (MO-11-10), one monzogabbro (MO-11-12), three monzodiorites (MO-11-13, MO-11-14, MO-11-21) and one monzonite (MO-11-26). Biotite concentrates alkali elements. In particular, Cs, Rb, and Ba concentrations are  $10^2$ - $10^3$  times primitive mantle values (Fig. 7b). Ba is especially concentrated in the phlogopites from the more primitive cumulates (e.g., 5798 ppm in one biotite from MO-10-392). Similarly, Sr is enriched in the biotites of the ultramafic cumulates. The Sr-enrichment is not present in the monzogabbros and monzodiorites, indicating that in these lithologies, Sr fractionates into feldspars. An enrichment of Pb, Zr, Hf, and notably Nb is present in biotites of all lithologies. Nb concentrations

generally increase with progressive fractionation from 4.6-9.1 ppm in the phlogopite wehrlites (though one phlogopite wehrlite (MO-10-394) has an average Nb concentration of 39.8 ppm Nb in biotite) to 32.3-78.4 ppm in the more evolved lithologies. The high concentrations on TiO<sub>2</sub>, Nb, Zr, and Hf are all in accordance with the compatibility of high field strength element (HFSE) in biotite. V is also highly compatible in biotite with concentrations varying between ~200-800 ppm.

#### Fe-Ti Oxides

Fe-Ti oxides first appear as minor fractionating phases in the phlogopite wehrlites, occurring as 50-200 μm subequant grains in between olivine, clinopyroxene, and phlogopite. The composition is dominated by magnetite-ülvospinel solid solution (Fig. 8a). Occasionally, oxides are enclosed by olivine, which exhibit minor chromitite substitution. Magnetite-ülvospinel<sub>solid-solution</sub> oxides persist as crystallizing phases into the phlogopite clinopyroxenites where they occur mainly enclosed by clinopyroxene. Oxides in the phlogopitite, more evolved monzogabbros and monzodiorites, and lamprophyre are predominantly members of the hematite-ilmenite solid solution, though some magnetite is also present (Fig. 8a).

#### Feldspars

Alkali-feldspar and plagioclase first crystallize in the biotite monzogabbro in patchy intergrowths. In the more evolved lithologies, plagioclase grows in smaller crystals around megacrysts of alkali-feldspar. Anorthite (An) contents of plagioclase are uniformly low, with plagioclases in monzogabbros and monzodiorites varying from An<sub>16</sub> to An<sub>44</sub> and those in monzonites to quartz monzonites between An<sub>13</sub> and An<sub>30</sub> (Fig. 8b). An contents in the rims of plagioclase are 1-2 mol.% lower than the cores. The alkali-feldspar generally has compositions of ~Or<sub>0.9</sub>Ab<sub>0.1</sub>. Only plagioclase (An<sub>29</sub> to An<sub>44</sub>) is present in the analyzed lamprophyre.

Trace element concentrations of both plagioclase and alkali-feldspar were determined for one monzogabbro (MO-11-12), three monzodiorites (MO-11-13, MO-11-14, MO-11-21), and one monzonite (MO-11-26). Trace element patterns of plagioclases and alkali-feldspar are generally similar, with the exception that alkali-feldspars are more enriched in LILEs and plagioclase is enriched in light to middle REEs (Fig. 7c). The LILEs are variably enriched in the K-feldspar with Ba generally displaying the most pronounced enrichment (380-1011 times primitive mantle). HREEs are significantly depleted (0.01-1 times primitive mantle) and Pb, Sr, and Eu are enriched with respect to LREE.

#### Apatite

Trace elements for apatite in one phlogopitite (MO-11-10), one monzogabbro (MO-11-12), three monzodiorites (MO-11-13, MO-11-14, MO-11-21), and one monzonite (MO-11-26) were analyzed. The apatites are LREE enriched (Ce<sub>N</sub>/Yb<sub>N</sub> = 28.4-60.4) (Fig. 7d). Apatites are generally depleted in Eu, Sr, Pb, Zr, and Hf. Prior and concurrent crystallization of titanite (CaTiSiO<sub>5</sub>), which is observed in both the ultramafic and more evolved lithologies of the fractionation sequence, could sequester Eu and Sr, depleting crystallizing apatite in these elements. Other notable depletions include Nb, Rb, & Ba,

indicating both the inability of apatite to incorporate large amounts of these elements (except for Ba, which can be accommodated in alforsite, a Ba-end member phosphate), but also the affinity of biotite for these three elements and K-feldspar for Rb & Ba (Pan and Fleet 2002).

### Amphibole

Amphibole is found as both a primary magmatic phase and as secondary metamorphic overgrowth on clinopyroxene. Metamorphic amphibole is actinolitic and will not be discussed further. In the biotite-dominated fractionation sequence amphibole appears in the crystallization sequence only in the more evolved feldspar-bearing lithologies (i.e., monzodiorites and monzonites). The composition of these amphiboles is dominantly magnesiohornblende. Mg#’s of the amphiboles vary from 56-67 in the monzodiorites to 48-56 in the monzonites. Trace elements analyses were done on three monzodiorites from the biotite-dominated fractionation sequence (MO-11-13, MO-11-14, MO-11-21). Primitive mantle-normalized trace element patterns of amphibole in the monzodiorites are characterized by enrichment in LREE over HREE ( $(La/Yb)_N = 2.7-4.5$ ). In addition, they display depletions in Sr, Pb, and Eu.

## Discussion

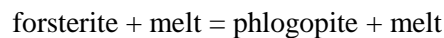
### Fractionation Sequence

There are several lines of field and petrographic evidence that indicate that the observed biotite-bearing lithologies could comprise a common plutonic cumulate sequence resulting from a single liquid line of descent. First, the contacts between the different plutonic rocks are gradational, with a general transition from more primitive to more evolved compositions from approximately northwest to southeast. Second, the poikilitic and orthocumulate textures observed in the phlogopite wehrlites and clinopyroxenites strongly suggest a cumulate origin (Fig. 5b,c,d). We therefore interpret the observed lithological variability to a primary fractionation sequence where the onset of crystallization of each phase is defined by the sequence olivine + clinopyroxene  $\rightarrow$  Fe-Ti oxides  $\rightarrow$  phlogopite + apatite  $\rightarrow$  k-feldspar + plagioclase + amphibole  $\rightarrow$  quartz. Notably, phlogopite is the dominant hydrous mafic mineral. In terms of lithology, this progression is manifested as wehrlites, to phlogopite wehrlites, to apatite-bearing phlogopite clinopyroxenites, to monzogabbros, to monzodiorites, and finally, to (quartz-)monzonites. Conspicuously, there are two large (km-scale) and many minor intrusions of red (alkali-)granites in close spatial proximity to the alkaline fractionation sequence. Field evidence is inconclusive to whether these intrusions are related to the fractionation sequence (primarily due to the fact that the contacts between the large red (alkali-)granite intrusions and the cumulate sequence are not readily exposed). Unpublished U-Pb zircon ages, however, indicate that these (alkali-)granites are significantly younger than the alkaline complex and are neither cogenetic nor contemporaneous with the biotite-dominated lithologies. We described them above for complete characterization of the observed plutonic igneous lithologies.

### Magmatic Biotite

There are multiple textural lines of evidence indicating that biotite is a primary magmatic phase.

Most importantly, there is a gradual decrease in biotite Mg# from the ultramafic lithologies to the more evolved lithologies. Continuity in composition (increases or decreases with Mg#) is also observed for minor and trace element, (e.g., Na<sub>2</sub>O, Cl, MnO, Ni, Cr). Further, in several samples, biotite is the dominant phase and reaches up to 1-2 cm, suggesting that it was a primary crystallizing phase. Its texture indicates that it is either an intercumulus or orthocumulate phase (subhedral to euhedral shape). In addition, no pervasive alteration of the cumulate sequence by a high or low temperature fluid is observed. Both clinopyroxene and biotite enclose small euhedral apatite prisms, indicating that they both continued to crystallize after apatite. Lastly, biotite is found in the widely documented melting reaction of olivine with a potassic melt with decreasing temperature (Barton and Hamilton 1979; Modreski and Boettcher 1972; Yoder and Kushiro 1969):



indicating a peritectic reaction that is most likely responsible for the exhaustion of olivine in the ultramafic cumulates with progressive fractionation.

#### Experimental Studies Relevant to the Dariv Fractionation Sequence

The majority of experimental crystallization studies performed on hydrous, high-K, mafic to ultramafic starting materials (leucitite, biotite mafurite, ugandite, madupite, basanite, lamprophyre, Di-Fo-Ks-Qz synthetic materials etc.) have found olivine + clinopyroxene + phlogopite ± spinel at multiple saturation (Edgar et al. 1980; Elkins-Tanton and Grove 2003; Esperança and Holloway 1987; Melzer and Foley 2000; Righter and Carmichael 1996). Only two studies obtained conditions conducive to orthopyroxene saturation and both required CO<sub>2</sub> to stabilize it (Edgar et al. 1980; Sato 1997). Apatite and sanidine have also been found as lower temperature, late crystallizing phases (Barton and Hamilton 1978; Barton and Hamilton 1979; Melzer and Foley 2000; Righter and Carmichael 1996). The phase relations determined by the experimental studies are generally consistent with the order of crystallization we have deduced for the biotite-dominated fractionation series of the Dariv Igneous Complex. The most important constraint that these experiments provide for the crystallization conditions of the Dariv biotite fractionation sequence is the temperature of the liquidus as it is broadly invariant (1100-1200°C) over a large range of pressures. Therefore, initial crystallization temperatures for the ultramafic cumulates were likely between 1100-1200°C. The liquidus mineralogy, however, can vary. In particular, the stability of olivine as a crystallizing phase in K-rich mafic melts is dependent on the reaction olivine + liquid → phlogopite + liquid (Yoder & Eugster, 1954; Yoder and Kushiro, 1969). High f<sub>H<sub>2</sub>O</sub>, P, H<sub>2</sub>O, and K<sub>2</sub>O contents will drive this reaction to the right (Esperança and Holloway 1987). This reaction is responsible for the shrinkage of the stability field of olivine in K-rich melts with increasing pressure and the decrease in olivine modal abundance with the appearance of phlogopite (Barton and Hamilton 1978; Barton and Hamilton 1979; Esperança and Holloway 1987; Righter and Carmichael 1996). As we observed a significant interval of olivine fractionation in Dariv (olivine Mg# 87 to 67), this suggests that pressures were not excessively high. The fact that no leucite was observed, however, suggests that pressures were

not below ~0.2 GPa. Therefore, these experimental studies indicate that the Dariv ultramafic lithologies crystallized from magmas at temperatures of 1,100-1200°C at pressures of >0.2 GPa. In the following section, we place more specific constraints on crystallization conditions using thermobarometers and oxygen barometers.

## Crystallization Conditions

### *Pressure and Temperature*

Thermometry based on major element clinopyroxene compositions (Putirka, 2008, eq. 32d) indicates that the phlogopite-bearing ultramafic and mafic rocks crystallized progressively over a temperature range of ~1210-1100°C (Table 13). This range of crystallization temperatures is in good agreement with experimental phase relations on high-K basaltic liquids (see discussion above). Pressure conditions of formation were approximated using the experimental Ba biotite-liquid equilibria of Righter & Carmichael, (1996). Ba concentrations of the melt in equilibrium with the most primitive analyzed phlogopite wehrlite, MO-10-394, were calculated using clinopyroxene Ba concentrations and the clinopyroxene-basalt partition coefficient of Hart & Dunn, (1993). Calculated Ba melt concentrations were slightly higher than that of mafic dikes with primitive compositions. Ultimately, a range of calculated Ba melt concentrations (1000-1500 ppm) for the primitive melt and the average Ba concentration (2220 ppm) in biotites from MO-10-394 were used in the calculations. Using the average clinopyroxene-thermometry temperature estimate for sample MO-10-394 (1206°C), the range of calculated pressure is 0.6 to 0.8±0.4 GPa.

For the more evolved rocks of the sequence, hornblende geochemistry was used to estimate temperature and pressure conditions of crystallization. The Al content in hornblende has been shown to increase with pressure, provided that quartz, K-feldspar, plagioclase, biotite, hornblende, titanite, and Fe-Ti oxides are also present as mineral phases in a rock (Hammarstrom and Zen 1986; Hollister et al. 1987; Schmidt 1992). Using the experimental calibrations of Schmidt, (1992) we calculated pressures of ~0.2-0.3 GPa using the Al-content of magnesio-hornblendes in the evolved rocks of the fractionation sequence. Temperature estimates using plagioclase-hornblende thermometry (Holland and Blundy 1994) yield temperature ranges of 642-726°C, which is close to the wet solidus of magmas which finally crystallize two feldspar+quartz assemblages. Slightly lower temperature estimates (538-672°C) were obtained from two-feldspar thermometry (Putirka 2008, Eq. 27a), indicating subsolidus re-equilibration of some feldspars.

The monzodiorites and monzonites are in a continuous, undeformed fractionation sequence with the ultramafic cumulates and spatial distances between the evolved and ultramafic cumulates (<1-5 km) allow for a pressure difference of 0.1-0.2 GPa. As there is significant uncertainty in estimated crystallization pressures of the ultramafic cumulates (e.g., the calibration of the Ba biotite-liquid exchange equilibrium has an error of 0.4 GPa and the liquid composition is calculated from cpx/melt Ba partition coefficients), crystallization pressures of 0.2-0.3 GPa for the evolved magmatic rocks and 0.3-0.5 GPa for

the ultramafic cumulates is consistent with geobarometric constraints and field observations.

Collaborative but indirect evidence for intrusion depths stems from the coexistence of brucite+serpentine in the serpentinites. As this mineral assemblage is limited to 360-390 °C (at 0.3-0.5 GPa) (Trommsdorff and Connolly 1996), its presence in the serpentinites indicates depths of <12-13 km (<0.34-0.38 GPa) assuming a typical continental geotherm of 30 °C/km. As arc geotherms are generally higher, this would provide a maximum depth limit.

### *Water Content of Melt*

The water content of a melt strongly controls both the types of mineral that it will crystallize and their order of crystallization. The hydrous minerals found in the alkaline fractionation sequence of Dariv, predominantly biotite, but also amphibole, require some water to crystallize. Although biotite can crystallize at fairly low H<sub>2</sub>O-contents (e.g., <0.5 wt.% H<sub>2</sub>O in a granodiorite with 67.51 wt.% SiO<sub>2</sub>), amphibole requires a minimum of 4 wt.% H<sub>2</sub>O at 0.2 GPa and 2.5 wt.% H<sub>2</sub>O at 0.8 GPa in the same magma (Naney 1983). The biotite-dominated fractionation sequence of Dariv suite does not display evidence for amphibole fractionation until relatively late (i.e., in the monzodiorites). This is consistent with the generally incompatible behavior of water in magmas which results in an increase in H<sub>2</sub>O content with differentiation. Further, an increase in water contents with progressive crystallization is supported by the widespread resorption and alteration of clinopyroxene to actinolitic hornblende in the monzonites and quartz monzonites. If we assume that at the onset of monzodiorite crystallization the melt achieved the minimum amount of water required to crystallize hornblende at 0.2-0.3 GPa (3.8 - 4.0 wt.% H<sub>2</sub>O), we can back-calculate the amount of water in the primitive melt parental to the cumulate sequence. If the primitive melt crystallized 40-50 wt.% (by mass) of biotite-bearing ultramafic and mafic cumulates which contain on average ~20 wt.% biotite (with 3-4 wt.% structurally bound H<sub>2</sub>O), and therefore ~0.6-0.8 wt.% H<sub>2</sub>O in the bulk cumulate, the primitive melt would need to contain ~2.2-2.6 wt.% H<sub>2</sub>O in order to saturate in amphibole when reaching the fractionation stage of the monzodiorites. Lower or higher H<sub>2</sub>O-contents in the primitive melt should lead to a later or earlier onset of amphibole crystallization, respectively. At 0.3-0.5 GPa, H<sub>2</sub>O-saturated basaltic melts contain ~6-8 wt.% in aqueous fluid. Therefore, the primitive melts of the biotite-dominated fractionation sequence were certainly hydrous, but not H<sub>2</sub>O-saturated.

### *Oxygen Fugacity*

The oxygen fugacity during crystallization of the biotite-dominated fractionation sequence can be estimated using various experimentally determined oxygen-barometers. Calculations using the olivine-orthopyroxene-spinel oxygen barometer of Ballhaus et al., 1991 yield  $f_{O_2}$  estimates of +1.8 to +3.2 ΔFMQ for the phlogopite wehrlites. As orthopyroxene is not present in the ultramafic lithologies of Dariv, we accounted for the effect of the shift in the activity of silica ( $a_{SiO_2}$ ) relative to orthopyroxene saturation on the  $f_{O_2}$  estimates using the formulations of O'Neill and Wall (1987) to calculate the  $a_{SiO_2}$  of olivine-



orthopyroxene equilibria and the estimates of  $a_{\text{SiO}_2}$  for typical melt compositions (Ghiorso & Carmichael, 1988). This correction resulted in a shift of -0.6 log units. In addition, vanadium (V) partitioning between melt and clinopyroxene can also be used to estimate  $f_{\text{O}_2}$  (Canil 2002; Canil and Fedortchouk 2000). The crystal structure of clinopyroxene preferentially incorporates  $\text{V}^{3+}$  over  $\text{V}^{4+}$  and  $\text{V}^{5+}$ , therefore,  $D_r^{\text{cpx/melt}}$  decreases with increasing  $f_{\text{O}_2}$ . Using V concentrations from analyses of primitive basaltic dikes (see “Composition of the Primitive, Parental Melt” section below) and measured V values in clinopyroxene from the most primitive analyzed wehrlite (MO-10-394), we calculated  $D_r^{\text{cpx/melt}}$ . Then, implementing experimentally determined relationships between  $D_r^{\text{cpx/melt}}$  and  $f_{\text{O}_2}$  (Canil and Fedortchouk 2000), we obtained estimates of +1.2 to +1.7  $\Delta\text{FMQ}$ . Both the olivine-spinel and the V-in-cpx oxygen barometers suggest that the Dariv ultramafic cumulates crystallized at elevated  $f_{\text{O}_2}$ 's. Other, subduction-related mafic alkaline magmas (phlogopite- and hornblende-bearing lamprophyres, shoshonites etc.) have also been observed to have particularly elevated  $f_{\text{O}_2}$ 's (+3 to +6 FMQ) compared to those of tholeiitic and calc-alkaline magmas (0 to +2 FMQ) (Carmichael 1991; Luhr and Carmichael 1981; Rowe et al. 2009; Vigouroux et al. 2008; Wallace and Carmichael 1989).

#### *In-situ Trace Element Modeling of Fractionation Mechanisms*

The gradual change in mineral modes across the fractionation sequence (i.e., from wehrlites to phlogopite- and apatite-rich clinopyroxenites to feldspar-bearing monzogabbros), indicating the accumulation of a progressively different fractionating mineral assemblage, and the steady decrease in Mg# of olivine, clinopyroxene, and biotite indicate that fractional crystallization was the dominant crystallization process in the formation of the ultramafic and mafic lithologies. To quantitatively assess the degree of differentiation ( $F$ ) and the amount of interstitial liquid ( $L$ ) trapped between cumulus minerals, we modeled the mineral trace element data following the method described by Hermann et al., (2001) based on the equations of Langmuir, (1989). In this model, we calculated mineral REE patterns starting from an average primitive melt composition (constrained from whole rock analyses of late-stage, co-genetic mafic dikes as discussed below).  $F$  and  $L$  are varied until a best fit to the measured REE data is obtained. This allows for assessment of both the degree of differentiation of a sample, of the amount of residual liquid in a cumulate, and whether some rocks represent true crystallized liquid compositions. For each observed and measured cumulate lithology, a best fit can be calculated with corresponding  $F$  and  $L$  values.

For the most ultramafic cumulates we modeled the mineral compositions of three phlogopite wehrlites (MO-10-392 (Mg# = 78.1), MO-10-323 (Mg# = 77.1), and MO-11-8 (Mg# = 76.3)) to capture the range of wehrlite fractionation. We also selected these samples because the constituent minerals do not show any zoning with respect to REEs, indicating that any trapped interstitial liquid present completely equilibrated with the cumulus phases. Clinopyroxenes from the most primitive analyzed wehrlite (MO-10-394) display some zoning, with the rims being 1.4-2.4 times enriched in REE as

compared to the cores. For this reason, this sample was not modeled. From the measured clinopyroxene-mineral  $K_D$  values, other mineral-melt partition coefficients were calculated and the model results were varied to obtain a best fit to the average clinopyroxene composition.

As REEs are more compatible and diffuse more rapidly in apatite than clinopyroxene at a given temperature (Cherniak 2000; Hart and Dunn 1993; Van Orman et al. 2001; Watson and Green 1981), the REE concentrations in apatite were used in the modeling for apatite-bearing lithologies. We selected one clinopyroxene-bearing phlogopite (MO-11-10), one monzogabbro (MO-11-13) and one monzodiorite (MO-11-14) to model. Due to the more “evolved” nature of the feldspar-bearing lithologies the primitive melt composition used to model the phlogopite wehrlites is inappropriate as a starting composition. Therefore, we used a model liquid composition that is in equilibrium with the mean composition of clinopyroxenes from the most evolved apatite-free wehrlite (MO-11-8). From the measured apatite-mineral  $K_D$  values, other mineral-melt partition coefficients were calculated and the model results were varied to obtain a best fit to the average apatite composition.

### *Results of Mineral Trace Element Modeling*

The *in situ* crystallization model reproduces the mineral trace element patterns of the phlogopite wehrlites when fractional crystallization is the dominant mechanism. The average clinopyroxene REE pattern of MO-10-392 is best fit when  $F = 63.5\%$  and  $L = 0.5\%$  (Fig. 9a), MO-10-323 when  $F = 67.3\%$  and  $L = 0.6\%$ , and MO-11-8 when  $F = 72\%$  and  $L = 0.5\%$ . The increase in the calculated degree of fractionation across the wehrlites is consistent with the decrease in the mineral  $Mg\#$ 's. The model results support the aforementioned evidence that the wehrlites are dominated by fractionated phases with insignificant amount of small interstitial liquid. Further, the mineral trace element patterns of the apatite-bearing phlogopite clinopyroxenite and the feldspar-bearing lithologies are also reproduced by a fractional crystallization model. Beginning with the new parental melt concentration at the onset of apatite crystallization (i.e. the melt composition at  $F = 72\%$  for the original primitive melt), the average apatite REE concentrations of the phlogopite (MO-11-10) are best produced when  $F = 29\%$  and  $L = 0\%$  (Fig. 9b), the monzogabbro (MO-11-13) when  $F = 44.5\%$  and  $L = 0.5\%$  (Fig. 9c), and the monzodiorite (MO-11-14) when  $F = 82.5\%$  and  $L = 0$ .

### Comparison to Phlogopite-Bearing Ultramafic Xenoliths

Xenoliths of lithologic similarity to the biotite-bearing cumulates of the Dariv Igneous Complex (i.e. phlogopite-bearing wehrlites and clinopyroxenites) have been found in high-K magmas from numerous localities (e.g. Eifel, Germany; Uganda; the Italian Volcanic Province; Sweet Grass Volcanics, Alberta & Montana; the Western Mexican Volcanic Belt) (Aoki and Kushiro 1968; Beccaluva et al. 2002; Buhlmann et al. 2000; Dawson and Smith 1992; Downes et al. 2004; Giannetti 1982; Giannetti and Luhr 1990; Righter and Rosas-Elguera 2001). In general, the xenoliths have been divided into two groups, 1) fragments of supra-subduction zone metasomatized mantle and 2) cumulates of high-K magmas. The first

group is identified by their typical deformation texture of mantle derived spinel peridotites, including porphyroclastic and coarse granular textures (e.g., Downes et al., 2004). Studies examining the mantle xenoliths have suggested that the high-K host magmas are produced through partial melting of metasomatized mantle and that the xenoliths are entrained fragments of this source region, (Ertan and Leeman 1996; Shaw and Eyzaguirre 2000). These studies propose that the phlogopite clinopyroxenites are created as veins or disseminated alteration by subsolidus metasomatism of a lherzolitic mantle by subduction zone fluids or melts rich in K, Ba, Rb, Sr, Ce, and water (Conticelli and Peccerillo 1992; Elkins-Tanton and Grove 2003; Wyllie and Sekine 1982). Other xenoliths have been interpreted as the products of crystal fractionation of high-K magmas similar to the alkali-basalts in which they are found (Aoki and Kushiro 1968; Buhmann et al. 2000; Downes et al. 2004; Righter and Rosas-Elguera 2001). This is supported by cumulate textures and a mineral chemistry similar to the phenocrysts in their host minettes. In addition, calculated REE patterns of melts in equilibrium with the clinopyroxenes in the xenoliths are very similar to those of the minettes (e.g., Downes et al. 2004) and both the xenoliths and the high-K lavas tend to have low  $\epsilon_{Nd}$  and radiogenic Sr signatures ( $\epsilon_{Nd} \approx -10$ ,  $^{87}Sr/^{86}Sr = 0.706-0.710$ ) (Buhmann et al. 2000; Farmer et al. 2002; Wannamaker et al. 2000). The Dariv ultramafic rocks are texturally and geochemically similar to this latter group of xenoliths. In most proposed scenarios, a previously enriched, mica-bearing mantle wedge above a subduction zone (represented by xenolith group 1) is remelted at a later time due to decompression melting or a heating event to produce the melts parental to the cumulates (xenoliths of group 2) (e.g., Downes et al. 2004; Righter and Rosas-Elguera 2001). Indeed, the occurrence of both groups of xenoliths (i.e. those representative of a metasomatized mantle wedge and those cumulative in origin) in the same lava flows or volcanic province suggests a closely linked origin. To assess whether the petrogenetic process described above is applicable to the Dariv Igneous Complex, we constrain the nature of the parental melts and the implication this has for their mantle source region in the following section.

#### Composition of the Primitive, Parental Melt

Primitive, syn-plutonic mafic dikes that cross cut the cumulate sequence (e.g., Fig. 4) have the appropriate composition to be parental to the cumulates. Several lines of evidence suggest that these dikes are late-stage, syn-plutonic dikes representative of a parental melt composition to the cumulates they intrude. First, the dikes have phenocryst and groundmass mineralogy similar to cumulates, namely biotite, clinopyroxene, and Fe-Ti oxides, secondly rounded enclaves, mineralogically identical to the mafic dikes are common in the monzodiorites and monzonites, and lastly the dike enclaves contain xenocrysts of minerals (quartz & k-feldspar) from the evolved granitoids (Fig. 3c). The first observation indicates that the dikes could have the appropriate composition to be parental to the cumulates. The latter two observations demonstrate that the mafic dikes were emplaced while the intrusions that lead to the cumulate sequence were still at relatively high temperatures, allowing for some mobilization of the mafic dikes and mingling with the evolved magma.

From whole rock geochemical analyses of dikes, primitive melt compositions were identified by the following chemical criteria: Mg# 65-75, Cr ~500-900 ppm, and Ni ~150-450 ppm. Four samples that met these constraints were identified. Accordingly, the range of their compositions might be representative of a primary primitive melt composition. This range in compositions corresponds to a near-primary, shoshonitic ( $\text{Na}_2\text{O} = 1.83\text{-}2.66$  wt.%,  $\text{K}_2\text{O} = 1.42\text{-}2.82$  wt.%) basalt to basaltic-andesite (49.8-53.3 wt.%  $\text{SiO}_2$ ) (Table 14). We used the clinopyroxene compositions of the most primitive analyzed phlogopite wehrlites (MO-10-394, MO-10-325, and MO-10-323) and known  $K_d$ 's to estimate trace element concentrations in the parental melt. The calculated compositions are in good agreement with the trace elements of the primitive mafic dikes, supporting the hypothesis that the dikes are indeed representative of a parental melt composition to the fractionation sequence (Fig. 10a).

### *Comparison to Primitive Arc Melts*

Both the calculated primitive melt compositions and those of the primitive dikes are highly enriched in Th, U, Ba, Rb, K, and LREE and have pronounced negative Nb-Ta depletion, geochemical hallmarks of subduction-zone related primitive magmas (Fig. 10a). Accordingly, a key question in this study is whether the Dariv primitive melt compositions are similar to primitive melt compositions generated at subduction zones and whether the fractionation sequence observed in Dariv may be common in other arcs. Using a global compilation of primitive melt compositions occurring in arcs from the GEOROC database (using the criteria Mg# = 0.65-0.79, Ni = 150-500, Cr = 250-1200), we compared the Dariv primitive melt compositions to those found in arcs. Arc lavas are dominated by tholeiitic and calc-alkaline compositions (Fig. 11a), but primitive andesites and alkaline basaltic primitive magmas also occur. Subduction zones generating primitive melts similar to that observed in Dariv, with higher  $\text{K}_2\text{O}$  and  $\text{K}_2\text{O}+\text{Na}_2\text{O}$  contents at similar  $\text{SiO}_2$  contents than calc-alkaline and tholeiitic arc basalts at similar  $\text{SiO}_2$  contents, are predominately continental arcs (e.g., Tonga/Kermadec, the Mexican Volcanic Belt, Honshu, Italy, the Andes, New Zealand, and Sunda/Banda) (Fig. 11). In addition, Dariv primitive melts are characterized by strong enrichments in LILE, LREE, Th, U, Pb, and Sr comparable to primitive continental calc-alkaline, high-K, and shoshonitic arc melts, significantly more enriched than primitive melts from calc-alkaline and tholeiitic oceanic arcs (Fig. 10b). In terms of other major element compositions, the Dariv primitive melt compositions are well within the range of observed values for primitive arc melt. Thus, the Dariv primitive melts appear to be most similar in composition to those found in continental arcs, suggesting that recycling of continental material plays an important role in their generation, most likely through subduction of weathered clastic sediments and the transfer of their geochemical signature into the mantle wedge. Although assimilation of crustal material during ascent through the overlying crust could help to produce the observed enrichments in incompatible elements, significant assimilation would dilute the primitive character of the melts, therefore we do not consider assimilation a significant process in the generation of the Dariv parental melts.

Compositions of high-K starting materials in experiments where olivine + phlogopite + clinopyroxene were found as crystallizing or residual phases are shown in Figure 15 for comparison. Although many of the starting materials have higher K<sub>2</sub>O, K<sub>2</sub>O+Na<sub>2</sub>O, and K<sub>2</sub>O/Na<sub>2</sub>O ratios than commonly observed in primitive arc basalts, several have compositions similar to that of the Dariv primitive melts. In particular, Sisson et al. (2005) found phlogopite + amphibole + plagioclase + apatite + titanomagnetite (+ minor olivine) to be in equilibrium with 18-29% melt of a starting material with the composition of a shoshonitic high-alumina basalt (AD19-93: K<sub>2</sub>O = 2.32; Na<sub>2</sub>O = 3.76). This composition (S05 in Figure 11) has similar alkali contents as the Dariv primitive basalts, suggesting that high-K calc-alkaline to shoshonitic primitive arc melts are capable of producing the evolved lithologies observed in Dariv through fractionation of SiO<sub>2</sub>-poor, biotite-rich cumulates.

### Modeling of the Subduction-Derived Component in the Primitive Melt Composition

Following our conclusion that the Dariv primitive melts are similar to high-K primitive melts found in continental arcs, we constrained the trace element characteristics of a slab-derived component contributing to the Dariv primitive melts. We followed the method of Grove et al., (2002) in which it is assumed that elements are contributed to a primitive melt either from melting of mantle peridotite or from a subduction-related H<sub>2</sub>O-rich component. The trace element concentration of the subduction component can be calculated from the following expression:

$$C_{PM} = C_{mantle} \left( 1 - \frac{X_{H_2O}}{\alpha} \right) + \left( \frac{X_{H_2O}}{\alpha} \right) \times C_{slab}$$

where  $C_{PM}$ ,  $C_{mantle}$ , and  $C_{slab}$  are the concentrations of the element of interest in the primitive melt, the melt that would result from melting an unmetasomatized mantle peridotite, and in the slab-derived component, respectively.  $X_{H_2O}$  is the weight fraction of water in the primitive melt and a proxy for the amount of slab component contribution.  $\alpha$  is a correction factor to account for the major element contribution of the slab-derived component. Grove et al., (2002) found that a correction of factor of ~0.6 was appropriate, therefore we used that value in our calculations.

In order to implement these calculations  $C_{mantle}$  and  $X_{H_2O}$  must be constrained. For  $C_{mantle}$  we implement a non-modal batch melting model (e.g., Shaw, 1970) to constrain the degree of partial melting of the mantle source. We start with a harzburgite depleted source composition (Grove et al. 2002) and incrementally melted the mantle to best reproduce the HREE element characteristics of the primitive melt composition. A best fit is obtained when 10% of partial melting occurs in the spinel field.  $X_{H_2O}$  was approximated using the estimated water concentrations for the Dariv primitive melts (~2.5 wt.% H<sub>2</sub>O). However, we calculated slab-derived components using a range of water concentrations (2.5-10 wt.%) in the primitive melt to investigate the range of potential slab component compositions.

## Results

The trace element composition of the slab-derived component is strongly enriched in LILE and LREE, and slightly enriched in HREE (Fig. 12a). The slab component accounts for 90-100% of the highly incompatible elements (Rb, Ba, Th, U, K, Nb, La, Ce, Pb, and Sr), 64-90% of the less incompatible elements (Nd, Zr, Hf, Sm, Eu, Gd), and 5-45% of the HREE (Fig. 12b). Compared to estimates of slab-derived component from Mt. Shasta in the Cascades (Grove et al. 2002), the Marianas Islands (Stolper and Newman 1994), and the Kohistan paleo-arc (Jagoutz et al. 2007), our calculated slab-component is comparable in absolute concentrations when  $X_{H_2O}$  is high (10 wt.%). Pre-eruptive water contents of 10 wt.% in primitive magmas are extremely high and likely represent the upper limit of H<sub>2</sub>O contents deduced for basaltic arc magmas with <6 wt.% H<sub>2</sub>O being a more common range for arc-related magmas (Grove et al. 2012). Further, our estimates for the Dariv primitive melts (2-3 wt.% H<sub>2</sub>O) are not compatible with such high water concentrations. This suggests that either the incompatible elements in the Dariv primitive melts reflect a particularly enriched subduction component or that an alternative model, where water and incompatible elements transfer to the primitive melt are decoupled in a two-stage process, must be considered. In the first scenario, high incompatible element concentrations in the slab component could be due to a particularly large contribution from subducted sediments. A particularly thick section of subducted sediment and/or high slab-top temperatures (during incipient subduction or tearing of the subducting slab) facilitating the transfer of subducted sediment into the mantle wedge could explain the strong enrichment in LILE, Th, U, K, and LREE observed in the Dariv subduction component.

In the second scenario, contribution of an incompatible element enriched component to the primitive melt would occur in two stages. First, a water- and incompatible-rich component could migrate from the slab progressively enriching a cold mantle wedge through the precipitation of phlogopite, amphibole, and potentially other hydrous phases. During this initial process H<sub>2</sub>O would be partly lost, whereas most of the incompatible elements would be retained in the crystallized phases. In a second step the mantle is reheated resulting in the melting of the previously precipitated hydrous phases and the production of an incompatible-element enriched, primitive melt with relatively low water contents. For the alkaline complex observed in the Dariv Range, we cannot yet discern between these two scenarios. Nevertheless, the close spatial occurrence of metasomatic and cumulative biotite-bearing ultramafic xenoliths from other localities with high-K magmas would seem to support the second scenario. In addition, high-K volcanics with biotite phenocrysts from other localities have been inferred to have formed through second-stage melting of a subduction-metasomatized mantle. For example, high-K basalts with subduction trace element patterns in the Sierra Nevada erupted in the Pliocene, well after Mesozoic-Cenozoic subduction ceased, and therefore must have been derived from melting of previously metasomatized mantle (Farmer et al. 2002; Van Kooten 1980). In addition, biotite-phenocrystic high-K basalts, lamprophyres, and basanites from the Western Mexican Volcanic Belt have very low B/Be ratios (indicating little direct input from slab-derived fluids into their source region), but elevated Ba/Ce and

other common measures of subduction zone trace element enrichment (Hochstaedter et al. 1996). This suggests that their genesis involved a multi-stage process whereby the high-K lavas were generated through later-stage melt of a metasomatized mantle selectively enriched in Ba (e.g., through precipitation of minerals such as biotite) (Foley 1992), instead of having formed through direct fluxing of subduction zone fluids. In both scenarios, a secondary remobilization event whether through lithospheric delamination and upwelling of hot asthenosphere (Ducea and Saleeby 1998; Farmer et al. 2002) or decompression (Hochstaedter et al. 1996) is required for their generation.

## CONCLUSION

The km-scale exposure of phlogopite- and clinopyroxene-dominated ultramafic lithologies of the Dariv igneous complex in Western Mongolia are remarkable in that they have hereto only been described as xenoliths in alkaline basalts. The range of high-K igneous rocks from phlogopite wehrlites to quartz monzonites of the Dariv Range provide an unparalleled opportunity to study the fractionation of a high-K arc-related primitive basalt. Detailed fieldwork and geochemistry suggests that the observed lithologies comprise a common fractionation sequence derived from a moderately hydrous, incompatible element-enriched primitive arc melt. Petrography and mineral chemistry indicate that fractional crystallization was the dominant mechanism in the formation of the observed lithologies. The ultramafic rocks crystallized at 0.3-0.5 GPa and 1200-1100°C. Estimates of water content and  $f_{O_2}$  of crystallization and an estimated parental melt composition indicate that the Dariv Igneous Complex formed due to the fractionation of a primitive high-K basalt with 2-3 wt.% H<sub>2</sub>O under conditions that were fairly oxidizing from the onset of crystallization ( $\geq$ FMQ+2). Comparison to a global dataset of primitive arc melts indicates that the primitive melts similar in composition to the Dariv primitive melts are common in continental arc settings. Modeling of the Dariv primitive melt in terms of a partial melt of a depleted mantle wedge and a slab-derived component indicates that the incompatible-element rich character of the Dariv primitive melt was likely due to either a particularly enriched subduction component or progressive enrichment of a cold supra-subduction zone mantle that was remelted at a later time.

## Acknowledgements

We thank Nilanjan Chatterjee for assistance with microprobe work, Markus Wälle for LA-ICPMS support, Uyanga Bold and Lkhagva-Ochir Said for helping to organize fieldwork logistics, Adam Bockelie and Yerenburged Munkhbold for their assistance in the field. We are grateful for many stimulating discussions with Francis MacDonald, Emily Smith, and Uyanga Bold concerning the tectonic history of the Altaids. Robert Luth and Tom W. Sisson provided thoughtful reviews of this manuscript. This work was supported by the National Science Foundation (grant number EAR-1322032).

## References:

Allan J, Carmichael I (1984) Lamprophyric lavas in the Colima graben, SW Mexico. Contributions to Mineralogy

and Petrology 88(3):203-216

Alonso-Perez R, Müntener O, Ulmer P (2009) Igneous garnet and amphibole fractionation in the roots of island arcs: experimental constraints on H<sub>2</sub>O undersaturated andesitic liquids. *Contributions to Mineralogy and Petrology* 157:541-558

Aoki Ki, Kushiro I (1968) Some clinopyroxenes from ultramafic inclusions in Dreiser Weiher, Eifel. *Contributions to Mineralogy and Petrology* 18(4):326-337

Armstrong JT (1995) Citzaf-a package of correction programs for the quantitative Electron Microbeam X-Ray-Analysis of thick polished materials, thin-films, and particles. *Microbeam Analysis* 4(3):177-200

Badarch G, Dickson Cunningham W, Windley BF (2002) A new terrane subdivision for Mongolia: implications for the Phanerozoic crustal growth of Central Asia. *Journal of Asian Earth Sciences* 21(1):87-110

Ballhaus C, Berry R, Green D (1991) High pressure experimental calibration of the olivine-orthopyroxene-spinel oxygen geobarometer: implications for the oxidation state of the upper mantle. *Contributions to Mineralogy and Petrology* 107(1):27-40

Barton M, Hamilton D (1978) Water-saturated melting relations to 5 kilobars of three Leucite Hills lavas. *Contributions to Mineralogy and Petrology* 66(1):41-49

Barton M, Hamilton DL (1979) The melting relationships of a madupite from the Leucite Hills, Wyoming, to 30 Kb. *Contributions to Mineralogy and Petrology* 69(2):133-142

Beccaluva L, Coltorti M, Di Girolamo P, Melluso L, Milani L, Morra V, Siena F (2002) Petrogenesis and evolution of Mt. Vulture alkaline volcanism (Southern Italy). *Mineralogy and Petrology* 74(2):277-297

Buhlmann AL, Cavell P, Burwash RA, Creaser RA, Luth RW (2000) Minette bodies and cognate mica-clinopyroxenite xenoliths from the Milk River area, southern Alberta: records of a complex history of the northernmost part of the Archean Wyoming craton. *Canadian Journal of Earth Sciences* 37(11):1629-1650

Buslov MM, Saphonova IY, Watanabe T, Obut OT, Fujiwara Y, Iwata K, Semakov NN, Sugai Y, Smirnova LV, Kazansky AY (2001) Evolution of the Paleo-Asian Ocean (Altai-Sayan Region, Central Asia) and collisions of possible Gondwana-derived terranes with the southern marginal part of the Siberian continent. *Geoscience Journal* 5(3):203-224

Canil D (2002) Vanadium in peridotites, mantle redox and tectonic environments: Archean to present. *Earth and Planetary Science Letters* 195(1):75-90

Canil D, Fedortchouk Y (2000) Clinopyroxene-liquid partitioning for vanadium and the oxygen fugacity during formation of cratonic and oceanic mantle lithosphere. *Journal of geophysical research* 105:26

Carmichael IS (1991) The redox states of basic and silicic magmas: a reflection of their source regions? *Contributions to Mineralogy and Petrology* 106(2):129-141

Cherniak D (2000) Rare earth element diffusion in apatite. *Geochimica et Cosmochimica Acta* 64(22):3871-3885

Conference Participants (1972) Penrose field conference on ophiolites. *Geotimes* 17:24-25

Coticelli S, Peccerillo A (1992) Petrology and geochemistry of potassic and ultrapotassic volcanism in central Italy: petrogenesis and inferences on the evolution of the mantle sources. *Lithos* 28(3,Äi6):221-240

Dawson JB, Smith JV (1992) Olivine-mica pyroxenite xenoliths from northern Tanzania: metasomatic products of upper-mantle peridotite. *Journal of Volcanology and Geothermal Research* 50:131-142

DeBari S, Kay SM, Kay RW (1987) Ultramafic xenoliths from Adagdak Volcano, Adak, Aleutian Islands, Alaska; deformed igneous cumulates from the Moho of an island arc. *Journal of Geology* 95(3):329-341



- Dijkstra AH, Brouwer FM, Cunningham WD, Buchan C, Badarch G, Mason PRD (2006) Late Neoproterozoic proto-arc ocean crust in the Dariv Range, Western Mongolia: a supra-subduction zone end-member ophiolite. *Journal of the Geological Society, London* 163:363-373
- Downes H, MacDonald R, Upton BGJ, Cox KG, Bodinier J-L, Mason PRD, James D, Hill PG, Hearn BC (2004) Ultramafic Xenoliths from the Bearpaw Mountains, Montana, USA: Evidence for Multiple Metasomatic Events in the Lithospheric Mantle beneath the Wyoming Craton. *Journal of Petrology* 45(8):1631-1662
- Ducea M, Saleeby J (1998) A case for delamination of the deep batholithic crust beneath the Sierra Nevada, California. *International Geology Review* 40(1):78-93
- Edgar AD, Condliffe E, Barnett RL, Shirran RJ (1980) An Experimental Study of an Olivine Ugandite Magma and Mechanisms for the Formation of its K-Enriched Derivatives. *Journal of Petrology* 21(3):475-497
- Elkins-Tanton LT, Grove TL (2003) Evidence for deep melting of hydrous metasomatized mantle: Pliocene high-potassium magmas from the Sierra Nevadas. *J Geophys Res* 108(B7):2350
- Ertan IE, Leeman WP (1996) Metasomatism of Cascades subarc mantle: Evidence from a rare phlogopite orthopyroxenite xenolith. *Geology* 24(5):451-454
- Esperança S, Holloway JR (1987) On the origin of some mica-lamprophyres: experimental evidence from a mafic minette. *Contributions to Mineralogy and Petrology* 95(2):207-216
- Farmer GL, Glazner AF, Manley CR (2002) Did lithospheric delamination trigger late Cenozoic potassic volcanism in the southern Sierra Nevada, California? *Geological Society of America Bulletin* 114(6):754-768
- Foley S (1992) Vein-plus-wall-rock melting mechanisms in the lithosphere and the origin of potassic alkaline magmas. *Lithos* 28(3):435-453
- Giannetti B (1982) Cumulate inclusions from K-rich magmas, Roccamonfina volcano, Italy. *Earth and Planetary Science Letters* 57(2):313-335
- Giannetti B, Luhr JF (1990) Phlogopite-clinopyroxenite nodules from high-K magmas, Roccamonfina Volcano, Italy: evidence for a low-pressure metasomatic origin. *Earth and Planetary Science Letters* 101:404-424
- Greene AR, DeBari SM, Kelemen PB, Blusztajn J, Clift PD (2006) A Detailed Geochemical Study of Island Arc Crust: the Talkeetna Arc Section, South-Central Alaska. *Journal of Petrology* 47(6):1051-1093
- Grove TL, Elkins-Tanton LT, Parman SW, Chatterjee N, Müntener O, Gaetani GA (2003) Fractional crystallization and mantle-melting controls on calc-alkaline differentiation trends. *Contributions to Mineralogy and Petrology* 145:515-533
- Grove TL, Parman SW, Bowring SA, Price RC, Baker MB (2002) The role of an H<sub>2</sub>O-rich fluid component in the generation of primitive basaltic andesites and andesites from the Mt. Shasta region, N. California. *Contributions to Mineralogy and Petrology* 142(4):375-396
- Grove TL, Till CB, Krawczynski MJ (2012) The role of H<sub>2</sub>O in subduction zone magmatism. *Annual Review of Earth and Planetary Sciences* 40:413-439
- Hammarstrom JM, Zen E-a (1986) Aluminium in hornblende: an empirical igneous geobarometer. *American Mineralogist* 71:1297-1313
- Hart SR, Dunn T (1993) Experimental cpx/melt partitioning of 24 trace elements. *Contributions to Mineralogy and Petrology* 113(1):1-8
- Hermann J, Müntener O, Günther D (2001) Differentiation of Mafic Magma in a Continental Crust-to-Mantle Transition Zone. *Journal of Petrology* 42(1):189-206
- Hochstaedter AG, Ryan JG, Luhr JF, Hasenaka T (1996) On B/Be ratios in the Mexican volcanic belt. *Geochimica*

et *Cosmochimica Acta* 60(4):613-628

Holland T, Blundy J (1994) Non-ideal interactions in calcic amphiboles and their bearing on amphibole-plagioclase thermometry. *Contributions to Mineralogy and Petrology* 116(4):433-447

Hollister LS, Grissom GC, Peters EK, Stowell HH, Sisson VB (1987) Confirmation of the empirical correlation of Al in hornblende with pressure of solidification of calc-alkaline plutons. *American Mineralogist* 72:231-239

Jagoutz O, Müntener O, Schmidt MW, Burg J-P (2011) The roles of flux- and decompression melting and their respective fractionation lines for continental crust formation: Evidence from the Kohistan arc. *Earth and Planetary Science Letters*

Jagoutz O, Müntener O, Ulmer P, Pettko T, Burg J-P, Dawood H, Hussain S (2007) Petrology and Mineral Chemistry of Lower Crustal Intrusions: the Chilas Complex, Kohistan (NW Pakistan). *Journal of Petrology* 48(10):1895-1953

Jagoutz O, Schmidt M (2012) The formation and bulk composition of modern juvenile continental crust: The Kohistan arc. *Chemical Geology* 298-99:79-96

Jagoutz OE (2010) Construction of the granitoid crust of an island arc. Part II: a quantitative petrogenetic model. *Contributions to Mineralogy and Petrology* 160:359-381

Kay SM, Kay RW (1985) Role of crystal cumulates and the oceanic crust in the formation of the lower crust of the Aleutian arc. *Geology* 13(7):461-464

Khain EV, Bibikova EV, Salnikova EB, Kröner A, Gibsher AS, Didenko AN, Degtyarev KE, Fedotova AA (2003) The Palaeo-Asian ocean in the Neoproterozoic and early Palaeozoic: new geochronological data and palaeotectonic reconstructions. *Precambrian Research* 122:329-358

Kozakov IK, Salnikova EB, Khain EV, Kovach VP, Berezhnaya NG, Yakoleva SZ, Plotkina YV (2002) Early Caledonian Crystalline Rocks of the Lake Zone in Mongolia: Formation History and Tectonic Settings as Deduced from U-Pb and Sm-Nd Datings. *Geotectonics* 36(2):156-166

Krawczynski MJ (2011) Experimental studies of melting and crystallization processes in planetary interiors. Massachusetts Institute of Technology

Langmuir CH (1989) Geochemical consequences of in situ crystallization. *Nature* 340(6230):199-205

Luhr JF, Allan JF, Carmichael IS, Nelson SA, Hasenaka T (1989) Primitive calc-alkaline and alkaline rock types from the Western Mexican Volcanic Belt. *Journal of Geophysical Research: Solid Earth* 94(B4):4515-4530

Luhr JF, Carmichael IS (1981) The Colima volcanic complex, Mexico: Part II. Late-quaternary cinder cones. *Contributions to Mineralogy and Petrology* 76(2):127-147

Maria AH, Luhr JF (2008) Lamprophyres, basanites, and basalts of the western Mexican volcanic belt: volatile contents and a vein-Åiwallrock melting relationship. *Journal of Petrology* 49(12):2123-2156

Melzer S, Foley SF (2000) Phase relations and fractionation sequences in potassic magma series modelled in the system CaMgSi<sub>2</sub>O<sub>6</sub>-KAlSi<sub>3</sub>O<sub>8</sub>-Mg<sub>2</sub>SiO<sub>4</sub>-SiO<sub>2</sub>-F<sub>2</sub>O, at 1 bar to 18 kbar. *Contributions to Mineralogy and Petrology* 138(2):186-197

Modreski PJ, Boettcher AL (1972) The stability of phlogopite + enstatite at high pressures; a model for micas in the interior of the Earth. *American Journal of Science* 272(9):852-869

Müntener O, Kelemen P, Grove T (2001) The role of H<sub>2</sub>O during crystallization of primitive arc magmas under uppermost mantle conditions and genesis of igneous pyroxenites: an experimental study. *Contributions to Mineralogy and Petrology* 141(6):643-658

Naney M (1983) Phase equilibria of rock-forming ferromagnesian silicates in granitic systems. *American Journal of*

Science 283(10):993-1033

Ownby SE, Lange RA, Hall CM (2008) The eruptive history of the Mascota volcanic field, western Mexico: age and volume constraints on the origin of andesite among a diverse suite of lamprophyric and calc-alkaline lavas. *Journal of Volcanology and Geothermal Research* 177(4):1077-1091

Pan Y, Fleet ME (2002) Compositions of the Apatite-Group Minerals: Substitution Mechanisms and Controlling Factors. *Reviews in Mineralogy and Geochemistry* 48(1):13-49

Putirka KD (2008) Thermometers and Barometers for Volcanic Systems. *Reviews in Mineralogy and Geochemistry* 69(1):61-120

Righter K, Carmichael ISE (1996) Phase equilibria of phlogopite lamprophyres from western Mexico: biotite-liquid equilibria and P-T; estimates for biotite-bearing igneous rocks. *Contributions to Mineralogy and Petrology* 123(1):1-21

Righter K, Rosas-Elguera J (2001) Alkaline Lavas in the Volcanic Front of the Western Mexican Volcanic Belt: Geology and Petrology of the Ayutla and Tapalpa Volcanic Fields. *Journal of Petrology* 42(12):2333-2361

Rowe MC, Kent AJR, Nielsen RL (2009) Subduction Influence on Oxygen Fugacity and Trace and Volatile Elements in Basalts Across the Cascade Volcanic Arc. *Journal of Petrology* 50(1):61-91

Rudnick RL, Fountain DM (1995) Nature and composition of the continental crust: A lower crustal perspective. *Rev Geophys* 33(3):267-309

Sato H (1977) Nickel content of basaltic magmas: identification of primary magmas and a measure of the degree of olivine fractionation. *Lithos* 10(2):113-120

Sato K (1997) Melting experiments on a synthetic olivine lamproite composition up to 8 GPa: Implication to its petrogenesis. *J Geophys Res* 102(B7):14751-14764

Schmidt MW (1992) Amphibole composition in tonalite as a function of pressure: an experimental calibration of the Al-in-hornblende barometer. *Contributions to Mineralogy and Petrology* 110:304-310

Sengör AMC, Natalín BA, Burtman VS (1993) Evolution of the Altaid tectonic collage and Palaeozoic crustal growth in Eurasia. *Nature* 364:299-307

Sengör AMC, Natalín BA, Burtman VS (1994) Tectonic evolution of Altaides. *Russian Geology and Geophysics* 35:33-47

Shaw CSJ, Eyzaguirre J (2000) Origin of megacrysts in the mafic alkaline lavas of the West Eifel volcanic field, Germany. *Lithos* 50(1,Äi3):75-95

Sisson TW, Grove TL (1993) Experimental investigations of the role of H<sub>2</sub>O in calc-alkaline differentiation and subduction zone magmatism. *Contributions to Mineralogy and Petrology* 113:143-166

Sisson TW, Ratajeski K, Hankins WB, Glazner AF (2005) Voluminous granitic magmas from common basaltic sources. *Contributions to Mineralogy and Petrology* 148:635-661

Stolper E, Newman S (1994) The role of water in the petrogenesis of Mariana trough magmas. *Earth and Planetary Science Letters* 121(3):293-325

Tatsumi Y, Shukuno H, Tani K, Takahashi N, Kodaira S, Kogiso T (2008) Structure and growth of the Izu-Bonin-Mariana arc crust: 2. Role of crust-mantle transformation and the transparent Moho in arc crust evolution. *J Geophys Res* 113(B2):B02203

Trommsdorff V, Connolly JA (1996) The ultramafic contact aureole about the Bregaglia (Bergell) tonalite: Isograds and a thermal model. *Schweiz Mineral Petrogr Mitt* 76(3):537-547

- Van Kooten GK (1980) Mineralogy, petrology, and geochemistry of an ultrapotassic basaltic suite, central Sierra Nevada, California, USA. *Journal of Petrology* 21(4):651-684
- Van Orman JA, Grove TL, Shimizu N (2001) Rare earth element diffusion in diopside: influence of temperature, pressure, and ionic radius, and an elastic model for diffusion in silicates. *Contributions to Mineralogy and Petrology* 141(6):687-703
- Vigouroux N, Wallace PJ, Kent AJ (2008) Volatiles in high-K magmas from the western Trans-Mexican Volcanic Belt: evidence for fluid fluxing and extreme enrichment of the mantle wedge by subduction processes. *Journal of Petrology* 49(9):1589-1618
- Villemant B (1988) Trace element evolution in the Phlegrean Fields (Central Italy): fractional crystallization and selective enrichment. *Contributions to Mineralogy and Petrology* 98(2):169-183
- Villemant B, Jaffrezic H, Joron J-L, Treuil M (1981) Distribution coefficients of major and trace elements; fractional crystallization in the alkali basalt series of Chaîne des Puys (Massif Central, France). *Geochimica et Cosmochimica Acta* 45(11):1997-2016
- Wallace P, Carmichael ISE (1989) Minette lavas and associated leucitites from the western front of the Mexican Volcanic Belt: petrology, chemistry, and origin. *Contributions to Mineralogy and Petrology* 103(4):470-492
- Wannamaker PE, Hulen JB, Heizler MT (2000) Early Miocene lamproite from the Colorado Plateau tectonic province, Southeastern Utah, USA. *Journal of Volcanology and Geothermal Research* 96(3,4):175-190
- Watson EB, Green TH (1981) Apatite/liquid partition coefficients for the rare earth elements and strontium. *Earth and Planetary Science Letters* 56:405-421
- Wyllie PJ, Sekine T (1982) The formation of mantle phlogopite in subduction zone hybridization. *Contributions to Mineralogy and Petrology* 79(4):375-380
- Yoder HS, Kushiro I (1969) Melting of a Hydrous Phase: Phlogopite. *American Journal of Science* 267-A:558-582

## FIGURE CAPTIONS

**Fig. 1** (a) Simplified map of the Central Asian Orogenic Belt (CAOB) and surrounding cratons. (b) Simplified terrane map of Mongolia. Notably, Mongolia consists of Pre-Cambrian autochthonous terranes surrounded by accreted allochthonous terranes, ophiolites, and island arc-related units to the South and West. The Dariv Range is located at the boundary of the Pre-Cambrian Altai Allochthon and the Lake Terrane. (c) Geological map of the Dariv Range based on field mapping, interpretation of Landsat images, and previously constructed maps of the area (Dijkstra *et al.*, 2006; Khain *et al.*, 2003). Our field mapping predominantly focused on the alkaline igneous sequences (both in the northwest and southeast parts of the Range) and the ophiolite sequence. See Supplementary Material for a map of the areas that the authors visited in the field.

**Fig. 2** (a) Geological map of detailed study area (see Fig. 1c for location) showing relationships between the Lake Terrane (the ophiolite sequence, the mantle section, the alkaline fractionation sequence, low grade metasediments), and the metamorphic Altai Allochthon. For legend with all lithologic units in the Dariv Range, see Fig. 1c. (b) Cross-section through Dariv Range showing the overall structure and relationship between various units. Profile location is indicated in Fig. 2a. Note that most contacts in this profile are of intrusive nature. The only two major faults are within the red (alkali-)granites.

**Fig. 3** Field photographs indicating field relationships. a) Intrusion of phlogopite-poor wehrlite in serpentinized mantle (sledgehammer is approximately 0.9 m long). b) Diffuse contact between monzonite and late stage aplite dike indicating comagmatic formation. Pencil is 15 cm long. c) Mafic dike inclusion (lamprophyre enclave) with K-feldspar xenocrysts in monzonite. Pencil is 13.5 cm long. d) Rounded biotite cumulate xenolith included in the monzonite, both of which are cross-cut by a late stage aplite dike. Rock hammer is 33 cm long.

**Fig. 4** Detailed cross-section across alkaline fractionation sequence. Clinopyroxene Mg#’s corresponding to distance along profile are given at top of figure. Lithologies become more evolved from left to right, starting with phlogopite wehrlites and grading into clinopyroxene-bearing monzonites. Contacts are drawn as sharp lines for clarity, but boundaries between lithologies are gradational. Profile location is indicated in Fig. 2a. Mineral abbreviations: ol – olivine, cpx – clinopyroxene, phl – phlogopite, ap – apatite, bt – biotite, ksp – K-feldspar, pl – plagioclase, hbl – hornblende, qtz – quartz.

**Fig. 5** Representative photomicrographs illustrating the studied fractionation sequence. Whole rock Mg# (unpublished data) are plotted in the upper right corners of the images. a, b, d, e, & h were taken in plane-polarized light, c was taken in cross polarized, and f & g are scanned thin section images. All thin sections except h (the alkali-feldspar granite) are 100  $\mu\text{m}$  thick. Mineral abbreviations are as in Fig. 4. a) Phlogopite wehrlite (MO-10-394) with minor phlogopite. Olivine shows irregular margins surrounded by phlogopite, reflecting reaction and consumption of primary olivine to form phlogopite. b) Phlogopite-rich wehrlite (MO-10-392) with increased modal percent of biotite. c) Phlogopite clinopyroxenite (MO-10-325) with interstitial biotite poikilitically enclosing subhedral clinopyroxenes. d) Clinopyroxene phlogopitite (glimmerite) (MO-11-10) with abundant and large apatite crystals. e) Biotite monzogabbro (MO-11-12) with biotite, clinopyroxene, and feldspar. f) Quartz-bearing monzodiorite (MO-11-14). g) Quartz monzonite (MO-11-26), notably clinopyroxene is still a fractionating phase. h) Red (alkali-)granite (MO-9-239).

**Fig. 6** Summary of individual analyses of olivine, clinopyroxene, and biotite major element compositions versus Mg#. Averages for samples are reported in the online Supplementary Material. Fields from other studies are based on data from lamprophyres (Allan and Carmichael, 1984; Carmichael *et al.*, 1996; Wallace & Carmichael, 1989; Carlier *et al.*, 1997; Luhr & Carmichael, 1981; Buhlmann *et al.*, 2000, Righter & Rosas-Elguera, 2001; Prelevic *et al.*, 2004; Maria & Luhr, 2008; van Bergen *et al.*, 1983), phlogopite-bearing dunite and wehrlite xenoliths (Downes *et al.*, 2004; Buhlmann *et al.*, 2000; Gianetti & Luhr, 1990; Aoki & Kushiro, 1968; Cid *et al.*, 2003) and experimentally crystallized minettes (Esperanca

& Holloway, (1987); Righter & Carmichael, (1996)). Solid black lines with arrow represents the average igneous trend determined from core compositions. In (d) and (e) the trend for metamorphic Tschermak exchange (Fe,Mg)<sub>2</sub>Si<sub>1</sub>Al<sub>1</sub> during cooling is shown by dashed red arrows. (a) Olivine NiO. (b) Olivine MnO. (c) Clinopyroxene TiO<sub>2</sub>. There is no systematic variation between cores and rims, rather TiO<sub>2</sub> concentrations appear to be related to local equilibration with Fe-Ti oxide. (d) Clinopyroxene Al<sub>2</sub>O<sub>3</sub>. (e) Biotite Al<sub>2</sub>O<sub>3</sub>. b) Biotite Na<sub>2</sub>O.

**Fig. 7** Average mineral trace element compositions normalized to primitive mantle (Sun & McDonough, 1989). 2 $\sigma$  inter-mineral variance of single samples are reported in the online Supplementary Material. a) Clinopyroxene cores. Legend given in (a) applies to b and d, as well. b) Biotite. c) Feldspar from monzogabbros, monzodiorites, and monzonites. K-feldspar data is shown in squares, plagioclase in diamonds. The lower dashed line indicated the LA-ICP-MS detection limit. d) Apatite.

**Fig. 8** (a) Individual analyses of Fe-Ti oxides on the FeO-TiO<sub>2</sub>-Fe<sub>2</sub>O<sub>3</sub> ternary. (b) Individual analyses of plagioclase and alkali-feldspar on an An-Ab-Or ternary diagram. Average feldspar compositions are reported in online Supplementary Material.

**Fig. 9** Primitive mantle normalized (Sun & McDonough, 1989) results from in-situ crystallization modeling following the approach of Hermann et al., (2001). Partition coefficients for clinopyroxene-melt were predominantly from Foley et al., (1996), however for several elements partition coefficients were taken from different studies (Nb, Pb, & Hf from Hart & Dunn, 1993; Th, U from Villemant et al., 1981) Apatite-melt partition coefficients are from Watson & Green (1981). (See online Supplementary Material for a compilation of partition coefficients used) . Modeling results suggest that fractional crystallization was the dominant mechanism and that essentially no interstitial liquid re-equilibrated with the clinopyroxene or apatite. Black filled symbols are the modeled mineral compositions and gray lines are actual mineral analyses. Results from the modeling of three samples are shown. a) Sample MO-10-392. Trace elements in clinopyroxene can be best explained 63% differentiation of a primitive alkaline melt. b) Sample MO-11-10 modeled with 29% differentiation of a melt in equilibrium with the most evolved phlogopite wehrlite with no modal apatite (i.e. the composition of the melt immediately before the onset of apatite fractionation.) c) A monzogabbro (MO-11-13) modeled with 44.5% differentiation, again starting from a more evolved melt composition as described in b.

**Fig. 10** Trace element composition of the estimated Dariv primitive melt. a) Average trace element concentration of melts calculated in equilibrium with clinopyroxenes from the three most primitive cumulate samples (Mg# of the clinopyroxene is given in parentheses), compared to the trace element composition of the four most primitive lamprophyre dikes (Table 3). (See Fig. 9 for a compilation of partition coefficients used) . b) Spider diagram for average compositions of MORB, primitive arc melts, and the primitive melt compositions from Dariv normalized to primitive mantle (Sun & McDonough, 1989). Average compositions of various continental and oceanic arcs are from the compilation described in text. Melts were characterized as low-K, calc-alkaline, high-K, or shoshonitic based on their K<sub>2</sub>O contents using the classification of Pecerrillo & Taylor (1976). Average MORB composition is from Kelemen et al., (2003). Solid line for each group indicates average. Shaded areas given for the Dariv primitive melts indicates the total range of analyzed compositions. Shaded areas for the average high-K continental arc and average tholeiitic oceanic arc show the 2 $\sigma_{SE}$  on averages. Other 2 $\sigma_{SE}$  ranges are omitted for clarity.

**Fig. 11** Major element data for compilation of primitive arc melts from the GEOROC database. Oceanic arcs are denoted in orange and continental arcs in blue. Dariv primitive melts are shown as dark green diamonds and their compositional range is represented with light green shading. High-K experimental starting materials where biotite was found as a crystallizing phase are indicated by red stars and the following labels. (**E76**: Edgar et al., 1976; **E78**: Edgar et al., 1978; **EH87**: Esperanca and Holloway, 1987; **RC96**: Righter & Carmichael, 1996; **ETG03**: Elkins-Tanton & Grove, 2003; **S05**: Sisson et al., 2005) (a) K<sub>2</sub>O v. SiO<sub>2</sub> with boundaries following (Pecerrillo & Taylor, 1976), (b) TAS diagram (Irvine & Baragar, 1976). Biotite-bearing high Mg# (>60) lavas are from the Sierra Nevadas (yellow circles) (Van

Kooten, 1980) and the Western Mexican Volcanic Belt (purple circles) (Allan & Carmichael (1984), Luhr & Carmichael (1981), Luhr et al. (1989), Wallace & Carmichael (1989), Carmichael et al. (1996), Righter & Carmichael (2001); Maria et al., (2008); Maria & Luhr (2008), Ownby et al. (2008), Vigouroux et al. (2008)).

**Fig. 12** Results from slab-component modeling. a) Primitive mantle normalized trace element diagram comparing the average Dariv parental melt composition (from whole rock analyses of syn-magmatic primitive mafic dikes), the calculated Dariv slab-derived component, the result of ~10% batch melting from a depleted source, and estimated slab-derived components from other arcs and paleo-arcs. Calculations of the slab-derived component are shown for 2.5, 5, and 10%  $X_{H_2O}$ . See text for further discussion. b) Fractional contribution of slab-derived component to the total primitive melt budget of individual trace elements.

Table 1: Summary of Analyzed Samples with GPS Locations and Modal Proportions of Minerals<sup>1</sup>

Sample #	Rock Type	GPS Location		Modal Proportion (%)						Accessory
		Longitude (E)	Latitude (N)	ol	cpx	bt	pl/ksp	amph	qtz	
MO-10-396	Phlog. Wehrlite	94°13'14"	46°38'59.1"	30	70	<2	-	-	-	
MO-10-394	Phlog. Wehrlite	94°13'50.8"	46°39'19.2"	20	75	5	-	-	-	
MO-10-322	Phlog. Wehrlite	94°12'6"	46°40'17.9"	20	50	30	-	-	-	
MO-9-248	Phlog. Wehrlite	94°15'17.6"	46°38'57.7"	15	60	25	-	-	-	Ap
MO-10-385	Phlog. Wehrlite	94°14'30"	46°39'22.4"	15	70	15	-	-	-	
MO-10-392	Phlog. Wehrlite	94°14'18.9"	46°39'19.6"	15	45	40	-	-	-	
MO-10-323	Phlog. Wehrlite	94°12'6"	46°40'17.9"	10	45	45	-	-	-	
MO-11-8	Phlog. Wehrlite	94°14'25.2"	46°39'10.2"	10	85	5	-	-	-	Cr-Spl, Mag, Usp
MO-10-325	Phlog. Cpxenite	94°12'6"	46°40'17.9"	-	70	30	-	-	-	Spn
MO-10-324	Phlog. Cpxenite	94°12'6"	46°40'17.9"	-	70	25	-	-	-	Spn, Ap, Zrn
MO-11-9	Phlog. Wehrlite	94°14'25.7"	46°39'10.8"	-	80	20	-	-	-	Ap, Mag, Usp
MO-11-10	Phlogopitite	94°14'25.9	46°39'10.8"	-	20	75	-	-	-	Ap (5%), Mag, Usp
MO-11-12	Monzogabbro	94°14'26.7"	46°39'10.7"	-	35	30	30	-	-	Ap, Zrn, Spn
MO-11-13	Monzogabbro	94°14'26.9"	46°39'11"	-	25	30	45	-	-	Ap, Zrn, Spn
MO-11-14	Monzodiorite	94°14'28.1"	46°39'11.2"	-	10	15	25/30	10	10	Ap, Hem, Ilm
MO-11-15	Monzodiorite	94°14'28.7"	46°39'11.2"	-	~5	15	30/30	15	10	Ap
MO-11-21	Monzonite	94°14'30.7"	46°39'12.1"	-	~5	15	30/20	15	15	Ap
MO-11-23	Monzonite	94°14'32.9"	46°39'12.4"	-	~5	10	40/20	10	15	Ap
MO-11-26	Qtz. Monzonite	94°14'34.6"	46°39'13.1"	-	~5	10	40/20	5	20	Spn
MO-10-386	Qtz. Monzonite	94°14'27"	46°39'18.9"	-	~5	15	40/20	10	15	Ap, Spn, Zrn
MO-11-19	Lamprophyre	94°14'29.8"	46°39'11.7"	-	5	50	45	-	-	Ap, Zrn, Hem

<sup>1</sup> Modal compositions have been approximated by a combination of thin section observation and image analysis.

Table 2: Comparison of temperature, pressure and oxygen fugacity calculated using different thermobarometers & oxygen barometers.

Reference: SAMPLE	TEMPERATURE (°C)			PRESSURE (GPa)	fO <sub>2</sub> (ΔFMO)	
	Clinopyroxene-Only Thermometer	Amphibole- Plagioclase Thermometer	Two Feldspar Thermometry	Al-in-hornblende barometer	Olivine-Spinel Oxygen Barometer	V in Cpx Canil & Fedortchouk (2000)
	Putirka (2008) eq. 32d <sup>a</sup>	Holland & Blundy (1994) <sup>b</sup>	Putirka (2008), Eq. 27b <sup>c</sup>	Schmidt (1992)	Ballhaus et al. (1991)	
MO-10-396	1206 ± 2 (n = 16)	-	-	-	-	-
MO-10-394	1195 ± 4 (n = 4)	-	-	-	3.90 ± 0.02 (n=11)	1.97 ± 0.37 (n = 4)
MO-10-385	1122 ± 27 (n = 2)	-	-	-	3.11 ± 0.01 (n = 9)	-
MO-10-392	1157 ± 16 (n = 8)	-	-	-	-	-
MO-10-323	1162 ± 4 (n = 10)	-	-	-	2.91 ± 0.16 (n = 7)	-
MO-11-8	1135 ± 24 (n = 3)	-	-	-	2.84 ± 0.21 (n = 7)	-
MO-11-9	1184 ± 5 (n = 6)	-	-	-	2.60	-
MO-10-325	1091 ± 37 (n = 10)	-	-	-	-	-
MO-10-324	1137 ± 20 (n = 8)	-	-	-	-	-
MO-11-10	1158 ± 12 (n = 4)	-	-	-	-	-
MO-11-12	1110 ± 23 (n = 5)	-	510-558	-	-	-
MO-11-13	1122 ± 12 (n = 3)	-	535-612	-	-	-
MO-11-14	-	693	546-648	0.152 ± 0.79 (n = 3)	-	-
MO-11-15	-	726	514-583	0.208 ± 0.50 (n = 5)	-	-
MO-11-21	-	702	528-548	0.199 ± 1.04 (n = 4)	-	-
MO-11-23	-	642	474-564	0.244 ± 0.51 (n = 3)	-	-
MO-11-26	-	682	474-533	0.154 ± 0.17 (n = 2)	-	-
MO-10-386	-	703	451-576	0.336 ± 0.17 (n = 8)	-	-

Errors are give as 2σ<sub>SE</sub> variation on averages of individual analyses.

<sup>a</sup> Calculated at 0.5 GPa for ultramafics and 0.3 GPa for feldspar bearing lithologies.

<sup>b</sup> Calculated at pressure of Al-in-hornblende of Schmidt (1992)

<sup>c</sup> Calculated at 0.3 GPa. Given ranges are the maximum calculated using various combinations of 1σ<sub>SD</sub> variations of average plagioclase and alkali-feldspar compositions.



Table 3: Primitive Dyke Compositions<sup>a</sup>

Sample #	MO-11-19	MO-9-228	MO-9-230	MO-9-263	Average	2 $\sigma_{SD}$
SiO <sub>2</sub>	48.69	52.92	50.29	50.10	50.50	3.53
TiO <sub>2</sub>	1.25	0.79	0.61	1.23	0.97	0.64
Al <sub>2</sub> O <sub>3</sub>	14.09	13.96	14.17	12.68	13.73	1.40
FeO	8.34	6.83	7.48	8.38	7.76	1.49
MnO	0.17	0.18	0.19	0.18	0.18	0.02
MgO	9.60	10.51	11.92	12.01	11.01	2.33
CaO	9.45	9.39	10.63	10.48	9.99	1.32
Na <sub>2</sub> O	2.60	2.13	1.82	1.89	2.11	0.70
K <sub>2</sub> O	2.76	2.13	1.63	1.41	1.98	1.19
P <sub>2</sub> O <sub>5</sub>	0.66	0.26	0.25	0.53	0.43	0.40
SrO	-	0.08	0.09	0.10	0.09	0.02
BaO	-	0.06	0.08	0.07	0.07	0.02
L.O.I.	1.49	-	-	-	-	-
Total	99.10	99.24	99.17	99.07	99.14	0.16
Mg#	67.24	73.28	73.96	71.87	71.59	6.05
Sc	22.8	23.9	29.3	25.6	25.4	5.7
V	197	132	188	152	167	60
Cr	520	643	642	643	612	122
Co	32.0	31.8	37.8	42.1	35.9	9.9
Ni	144	166	171	277	189	120
Cu	16.9	3.18	13.7	39.9	18.4	30.9
Zn	66.9	57.5	64.1	62.1	62.6	7.9
Rb	75.6	76.5	61.8	30.6	61.1	42.9
Sr	1181	614	772	785	838	483
Y	26.1	19.6	19.6	24.8	22.5	6.8
Zr	264	125	89.9	188	167	153
Nb	16.3	8.32	3.25	15.2	10.8	12.2
Sn	2.14	2.52	9.42	9.59	5.92	8.28
Cs	1.39	1.76	2.34	0.749	1.56	1.34
Ba	1007	561	729	684	745	377
La	59.0	29.8	38.3	45.8	43.2	24.8
Ce	124	62.0	77.0	90.7	88.4	53
Pr	14.8	7.14	9.06	11.1	10.5	6.5
Nd	59.9	28.3	38.9	45.6	43.2	26.5
Sm	10.5	5.25	7.18	8.59	7.89	4.5
Eu	2.64	1.40	1.76	1.98	1.94	1.04
Gd	7.74	4.68	5.68	6.93	6.26	2.70
Tb	1.03	0.63	0.72	0.86	0.81	0.35
Dy	5.11	3.59	3.84	4.77	4.33	1.46
Ho	0.928	0.739	0.761	0.902	0.833	0.192
Er	2.22	2.19	2.03	2.74	2.30	0.62
Tm	0.298	0.237	0.312	0.330	0.294	0.081
Yb	2.01	1.52	1.87	2.26	1.91	0.62
Lu	0.312	0.256	0.274	0.307	0.287	0.054
Hf	6.04	3.27	2.13	4.55	4.00	3.36
Ta	0.988	0.529	0.185	0.928	0.658	0.750
Pb	7.86	4.86	2.39	6.52	5.41	4.71
Th	7.48	7.44	7.93	6.75	7.40	0.97
U	1.89	1.82	1.75	1.26	1.68	0.57

<sup>a</sup>Major elements oxides are given wt.%. Trace elements are given in ppm.